New magnetic fabric data and their comparison with palaeostress markers in the Western Fars Arc (Zagros, Iran): tectonic implications

Charles Aubourg, Brigitte Smith, Ali Eshraghi, Olivier Lacombe, Christine Authemayou, Khaled Amrouch, Olivier Bellier and Frédéric Mouthereau

Geological Society, London, Special Publications 2010; v. 330; p. 97-120
doi:10.1144/SP330.6

New magnetic fabric data and their comparison with palaeostress markers in the Western Fars Arc (Zagros, Iran): tectonic implications

CHARLES AUBOURG[1]*, BRIGITTE SMITH[2], ALI ESHRAGHI[3], OLIVIER LACOMBE[4], CHRISTINE AUTHEMAYOU[5], KHALED AMROUCH[4], OLIVIER BELLIER[6] & FRÉDÉRIC MOUTHEREAU[4]

[1]*Géosciences & Environnement Cergy, Université Cergy Pontoise, CNRS, 5, mail Gay Lussac, Neuville-sur-Oise, 95031 Cergy, France*

[2]*Géosciences Montpellier, Université de Montpellier 2, CNRS, Place Eugène Bataillon, 34095 Montpellier, France*

[3]*Geological Survey of Iran, Tehran, Iran*

[4]*Laboratoire de Tectonique, Université P. et M. Curie-Paris 6, CNRS, Paris, France*

[5]*Laboratoire Domaines Océaniques, CNRS, Institut Universitaire Européen de la Mer, Université de Brest, Place Nicolas Copernic, 29280 Plouzane, France*

[6]*CEREGE – UMR CNRS 6635 – Aix – Marseille Université, BP 80, Europôle, Méditerranéen de l'Arbois, 13545 Aix-en-Provence, Cedex 4, France*

**Corresponding author (e-mail: aubourg@u-cergy.fr)*

Abstract: The Zagros Simply Folded Belt (ZSFB) is an active fold-and-thrust belt resulting from the still continuing continental collision between the Arabian plate and the Iranian plate, which probably started in the Oligocene. The present-day shortening (N25°) is well documented by focal mechanisms of earthquakes and global positioning system (GPS) surveys. We propose in this study a comparison of published palaeostress markers, including magnetic fabric, brittle deformation and calcite twinning data. In addition, we describe the magnetic fabric from Palaeocene carbonates (10 sites) and Mio-Pliocene clastic deposits (15 sites). The magnetic fabrics are intermediate, with magnetic foliation parallel to the bedding, and a magnetic lineation mostly at right angles to the shortening direction. This suggests that the magnetic fabric retains the record of an early layer-parallel shortening (LPS) that occurred prior to folding. The record of LPS allows the identification of originally oblique folds such as the Mand Fold, which have developed in front of the Kazerun Fault. The shape parameter of the magnetic fabric indicates a weak strain compatible with the development of detachment folds in the ZSFB. The palaeostress datasets, covering the Palaeocene to Pleistocene time interval, support several folding episodes accompanied by a counter-clockwise rotation of the stress field direction. The Palaeocene carbonates in the ZSFB record a N47 LPS during early to middle Miocene detachment folding in the High Zagros Belt (HZB). The Mio-Pliocene clastic deposits recorded a N38 LPS prior to and during detachment folding within the ZSFB at the end of the Miocene–Pliocene. Similarly, fault slip and calcite twin data from the ZSFB also support a counter-clockwise rotation from NE to N20 between the pre-folding stage and the late rejuvenation of folds. This counter-clockwise trend of palaeostress data agrees with fault slip data from the HZB. During the late stage of folding in the ZSFB, the Plio-Quaternary palaeostress trends are consistently parallel to the present-day shortening direction.

In the Zagros active fold-and-thrust belt, the present-day stress and strain fields are now well constrained by geodetic and seismic data (Tatar *et al.* 2002; Talebian & Jackson 2004; Hessami *et al.* 2006; Lacombe *et al.* 2006; Walpersdorf *et al.* 2006). It is, however, also important to elucidate the stress pattern in the different stages of fold-and-thrust belt formation, from layer-parallel shortening (LPS) to folding and thrusting. Palaeostress or -strain can be determined by several means, including analyses of magnetic fabric, striated microfaults and calcite twinning.

From: LETURMY, P. & ROBIN, C. (eds) *Tectonic and Stratigraphic Evolution of Zagros and Makran during the Mesozoic–Cenozoic*. Geological Society, London, Special Publications, **330**, 97–120.
DOI: 10.1144/SP330.6 0305-8719/10/$15.00

The objectives of this work are the following. We will first characterize the general pattern of the magnetic fabric in the western Fars Arc, based on new data combined with previously published data. Then we will compare this information with the Late Cenozoic palaeostress data deduced from analyses of both small-scale deformation recorded in the field and calcite twinning. Finally, we will integrate the Late Cenozoic stress pattern in a comprehensive scheme of the tectonic evolution of the Fars.

Palaeostress markers in fold-and-thrust belts

Magnetic fabric is analysed from the measurement of standard cores of *c*. 10 cm^3. In essence, the magnetic fabric averages the 3D preferred orientation of billions of magnetic grains with anisotropy as small as 0.1% (Hrouda 1982). In unmetamorphosed rocks from fold-and-thrust belts, the magnetic fabric generally integrates the record of burial and subsequent deformation (Graham 1966; Hrouda 1982; Borradaile 1987) (Fig. 1). Numerous studies in fold-and-thrust belts have shown that magnetic fabric, when measured with the anisotropy of low-field magnetic susceptibility (AMS), can be used successfully as a record of layer-parallel shortening (LPS), thus behaving as a good proxy for strain (Graham 1966; Kissel *et al.* 1986; Averbuch *et al.* 1992; Hirt *et al.* 1995; Aubourg *et al.* 1997; Parés *et al.* 1999). Generally, the magnetic lineation from AMS (K_1) lies at right angles to the LPS direction whereas the magnetic foliation (the plane containing AMS K_1 and K_2 axes) remains parallel to the bedding. This fabric is labelled 'intermediate fabric' according to the nomenclature proposed by Averbuch *et al.* (1992). When rocks are more strained, the bedding-related magnetic foliation is progressively lost and a tectonic-related magnetic foliation may develop. This fabric is called 'tectonic fabric'. It should be noted that tectonic-related magnetic foliation can develop without its counterpart being visible in the field (such as a cleavage). Several pioneering studies envisaged the quantitative issue of AMS by using appropriate parameters (see the review by Borradaile 1987). However, it appears that, in addition to strain, the nature of magnetic carriers of AMS controls also the magnitude of AMS parameters (Rochette *et al.* 1992; Hrouda *et al.* 1993). Despite this complication, the shape parameter *T* (Jelinek 1981) may provide a valuable indication of the progressive loss of bedding-parallel magnetic foliation during the imprint of LPS in sedimentary rocks from fold-and-thrust belts (Parés *et al.* 1999).

The occurrence of intermediate or tectonic magnetic fabric is apparently dependent on the efficiency of the décollement level and the nature of the sedimentary rocks (Frizon de Lamotte *et al.* 2002). Several researchers observed that claystones, carbonates and clastic deposits have developed distinct magnetic fabrics in response to similar strain history (Bakhtari *et al.* 1998; Sagnotti *et al.* 1998). It is easier to develop a tectonic fabric in carbonates and clastic deposits compared with claystones, where magnetic foliation is strongly controlled by the bedding. When the décollement level is frictionless, as it may be in salt-based thrust belts, intermediate LPS fabric is dominant (Parés *et al.* 1999; Kanamatsu *et al.* 2001). However, when the décollement level has high friction, tectonic LPS fabrics are likely to develop (see discussion by Robion *et al.* 2007). During folding, we may distinguish between detachment folds and fault-related folds.

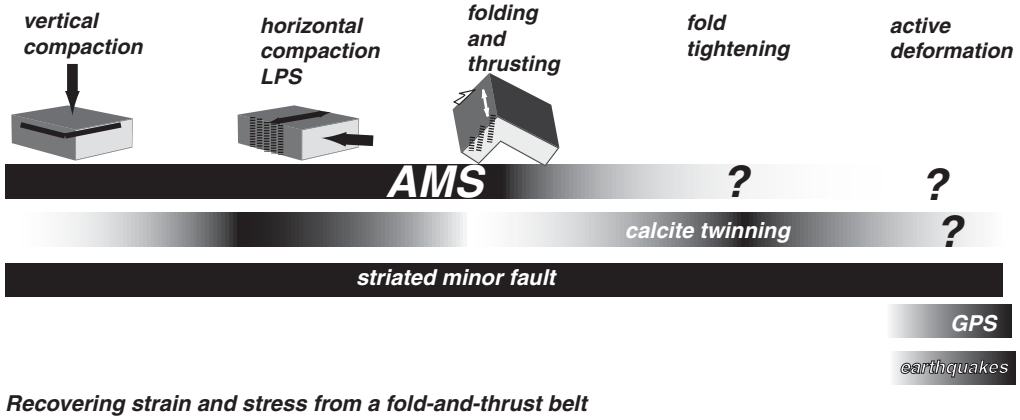

Fig. 1. Record of palaeostress in fold-and-thrust belt by several techniques, all used in this study. Dark shading indicates the timing of the palaeostress record.

In the case of a detachment fold, the strain is weak and the LPS-related magnetic fabric is generally preserved (Aubourg *et al.* 2004). In contrast, when the strain is more pronounced, as it is in a fault-propagation fold, a fold-related magnetic fabric can develop (Saint-Bezar *et al.* 2002) (Fig. 1). The strain imprint by AMS in the later stage of fold-and-thrust belt formation as fold tightening and active deformation occurs is not yet well documented. Hamilton *et al.* (2004) envisaged the record of post-folding strain by AMS in thrust belts.

The analysis of small-scale brittle deformation is performed directly in the field. This consists of inverting fault slip data into stress tensors representative of the fault population (Angelier 1990; Mercier *et al.* 1991). Generally, several tens of striated minor faults are analysed to compute a palaeostress tensor, including the orientations of the three principal stress axes σ_1, σ_2 and σ_3 and the stress ellipsoid shape ratio Φ defined as $\Phi = (\sigma_2 - \sigma_3)/(\sigma_1 - \sigma_3)$. This now classical approach has given rise to many theoretical developments and successful applications over the last 30 years, so there is no need to enter into much detail here [refer to Authemayou *et al.* (2006) and Lacombe *et al.* (2006) for basic assumptions, limitations and references on this technique]. To provide time constraints on palaeostress data, several criteria are used such as the age of faulted rocks, the eventual superimposition of striations along the fault plane and the orientation of palaeostress axes with respect to bedding, in addition to evidence of syntectonic sedimentation when available. In favourable situations, it is possible to recover the whole palaeostress story of the thrust belt, from burial to active deformation (Fig. 1).

Mechanical e-twinning readily occurs in calcite deformed at low temperature (Burkhard 1993). Calcite twinning requires a low critical resolved shear stress (CRSS), which depends on grain size (Rowe & Rutter 1990) and internal twinning strain, and has only a slight sensitivity to temperature, strain rate and confining pressure; thus calcite twinning fulfils most of the requirements for palaeopiezometry (Lacombe 2007). In this paper, we used Etchecopar's method of inverting calcite twin data (Etchecopar 1984; see details given by Lacombe 2001, 2007). This method applies to small twinning strain that can be approximated by coaxial conditions, so orientation of twinning strain can be correlated with palaeostress orientation (Burkhard 1993). Calcite twinning analysis is performed optically under a U-stage microscope. From mutually perpendicular thin-sections, tens of calcite grains are analysed for a sample at a given site, from host rock matrix and/or veins. The inversion process takes into account both the twinned and the untwinned planes, the latter being those of the potential e-twin planes that never experienced a resolved shear stress of sufficient magnitude to cause twinning. The inverse problem consists of finding the stress tensor that best fits the distribution of twinned and untwinned planes. As for fault slip data, the orientations of the three principal stresses σ_1, σ_2, and σ_3 are calculated, together with the Φ ratio, but in addition the peak differential stress $(\sigma_1 - \sigma_3)$ is also computed. If more than *c.* 30% twinned planes in a sample are not explained by a unique stress tensor, the inversion process is repeated with the uncorrelated twinned planes and the whole set of untwinned planes. Where polyphase deformation has occurred, this process provides an efficient way of separating superimposed twinning events. The stress inversion technique is to date the only technique that allows simultaneous calculation of principal stress orientations and differential stress magnitudes from a set of twin data, and that therefore allows differential stress magnitudes to be related unambiguously to a given stress orientation and stress regime (Lacombe 2007). To date the palaeostress tensor derived from calcite twinning data we have to take into account the age of rocks, the various generations of calcite veins and the orientation of palaeostress axes with respect to bedding. It is generally assumed that calcite twinning records early LPS (Craddock & van der Pluijm 1999) but several studies have also reported the potential of calcite twinning to record late-stage fold tightening strain (Fig. 1; Harris & van der Pluijm 1998; Lacombe 2001; Lacombe *et al.* 2007).

Geological setting

The Zagros belt is one of the youngest continental collision belts, resulting from the convergence between the Arabian and the Iranian plates (Fig. 2a). The subduction started in the late Jurassic and the continental collision began by the Late Oligocene–Miocene. Geodetic data show that about one-third of the total *c.* 22 mm a^{-1} present shortening between Arabia and Eurasia is accommodated in the external part of the Zagros (Fig. 2b). The Zagros comprises two major NW–SE-trending structural zones, the High Zagros Belt (HZB) and the Zagros Simply Folded Belt (ZSFB) (Fig. 2c). They are bounded by two major thrusts: the Main Zagros Thrust (MZT), which is the inactive suture between the Arabian plate and the Iranian plate (Ricou *et al.* 1977; Berberian 1995), and the High Zagros Thrust (HZT), which marks the NE boundary of the Arabian passive palaeomargin. We limit the presentation of these units to the central Zagros, bracketed between the longitudes 51° and 55°E, where the ZSFB corresponds to the Fars Arc (Fig. 2c). In this study we use the fault

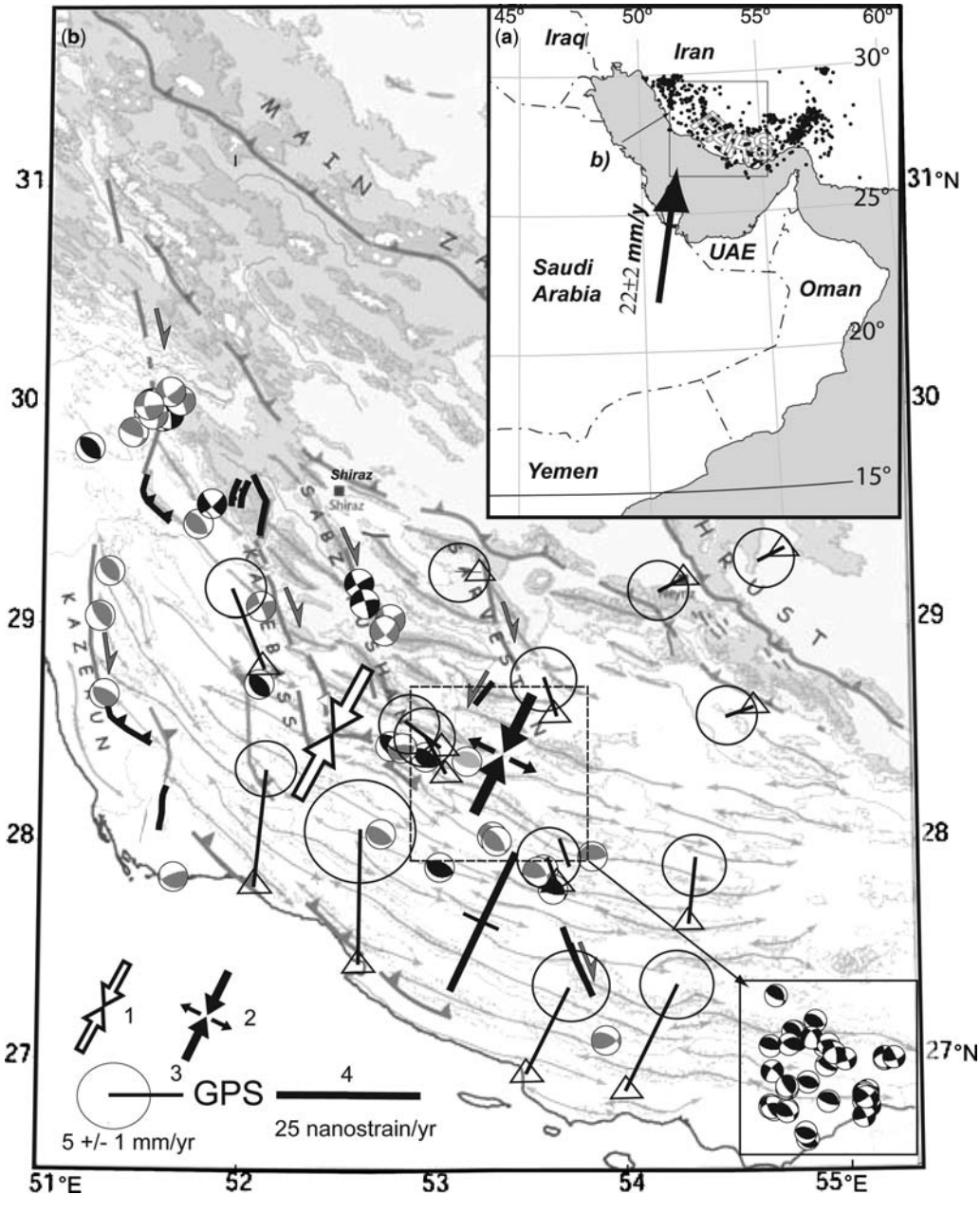

Fig. 2. Present-day deformation and structure of the Fars Arc. (**a**) View of the Arabian plate and the Zagros, marked by a pervasive seismicity. (**b**) Present-day deformation as indicated by seismicity and GPS displacement. Shortening directions inferred from the inversion of earthquake focal mechanisms. 1 and 2, current compressional trend derived from moderate earthquakes and microearthquakes, respectively (Lacombe *et al.* 2006). 3 and 4, GPS velocity field relative to central Iran and related strain rate, respectively (Walpersdorf *et al.* 2006). (**c**) Main tectonic structures of the High Zagros Belt and the Zagros Simply Folded Belt in the setting of Arabian and Iranian plate convergence. The disposition of major blind thrusts (High Zagros Fault, Mountain Front Fault, and Zagros Front Fault) along the Kazerun Fault (KZ) in the western Fars Arc and their intersection in the Eastern Fars Arc should be noted. K, Karehbass Fault; ZMS, Zagros–Makran Syntaxis. We indicate the location of the Mand and Minab anticlines at the western and eastern tips of the Fars Arc, respectively. The magnetic fabric of these anticlines is shown in Figure 6.

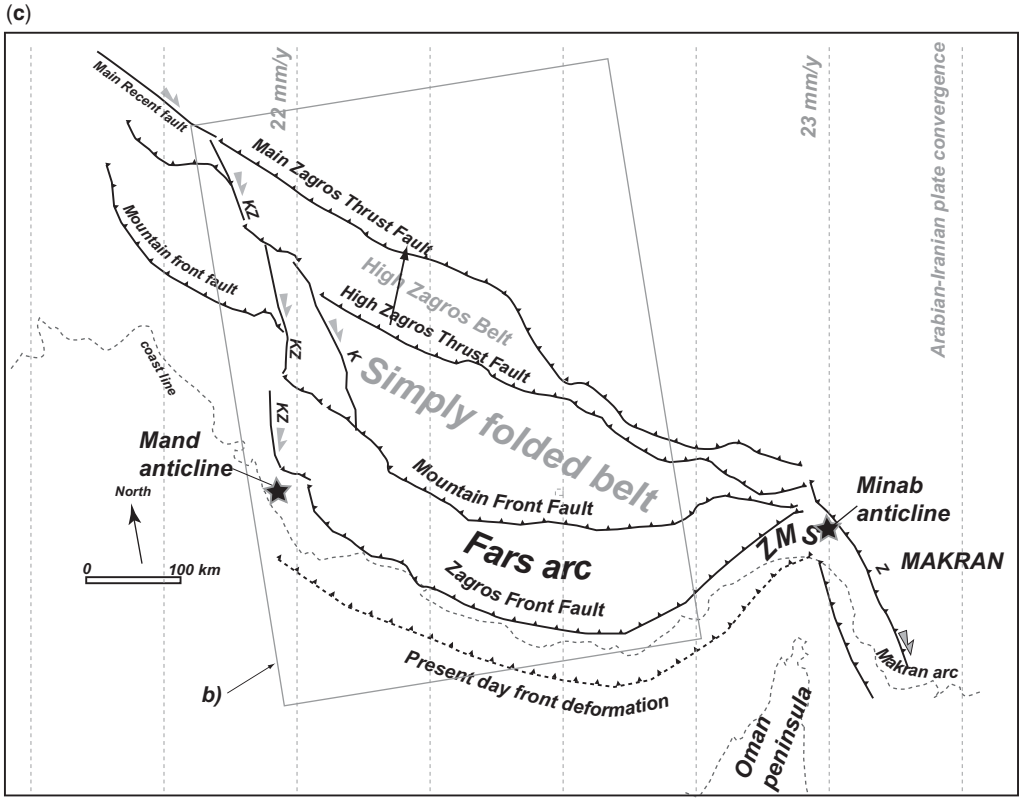

Fig. 2.

nomenclature proposed by Sepehr & Cosgrove (2004) & Sherkaty & Letouzey (2004). The ZSFB is bounded by the High Zagros Thrust to the NE and the Zagros Front Fault to the SW. It should be noted that a blind and active thrust, the Mountain Front Fault (MFF) is localized in the intermediate part of ZSFB. The MFF coincides approximately with the 1500 m topographic contour map and major zone of seismicity (Sepehr & Cosgrove 2004).

The HZB is the most uplifted (up to 4000 m) and eroded part of the Zagros mountain belt. However, its present-day seismic activity is low (Talebian & Jackson 2004). The main folding stage started during the Late Oligocene–Early Miocene and ended in the late Miocene (Sherkati *et al.* 2005). Navabpour *et al.* (2007) documented successive palaeostress fields in the central HZB (Shiraz area) using tectonic analysis of small-scale brittle deformation. They reported a *c*. 50° counter-clockwise rotation of the palaeostress field from the Late Oligocene–Early Miocene (*c*. N53°) to Quaternary (*c*. N2°). They proposed that this counter-clockwise rotation of the palaeostress field reflects large-scale plate kinematic changes (McQuarrie *et al.* 2003). The reconstructed compressional trends are reported in Figure 2b.

In contrast to the inactive HZB, the ZSFB is seismically active (Berberian 1995) and it concentrates *c*. 40% of the convergence between the Arabian and Iranian plates (Tatar *et al.* 2002). Most of the earthquakes take place in the upper part of the basement (at 11–15 km depth) (Tatar *et al.* 2004). A large part (*c*. 95%) of the deformation is thus accommodated aseismically by creep on faults and folding in the cover (Masson *et al.* 2005). Using balanced cross-sections, several studies bracketed the total shortening between 25 and 37 km in the Fars Arc (Blanc *et al.* 2003; Molinaro *et al.* 2003, 2004*a*, *b*; McQuarrie 2004; Sherkati & Letouzey 2004; Sherkati *et al.* 2006; Mouthereau *et al.* 2007*a*, *b*). Both basement and the *c*. 10 km of Palaeozoic to Cenozoic cover are involved in collisional shortening. Folding is still continuing, as Quaternary fold growth is commonly observed along the coast of the Fars Arc (Homke *et al.* 2004; Oveisi *et al.* 2007). The Kazerun Fault (Berberian 1995) laterally

bounds the Fars Arc along its SW margin. The Kazerun Fault has been studied by Authemayou *et al.* (2006), and its satellite faults (Fig. 2b), the Karehbass, Sabz Pushan and Sarvestan faults, by Berberian (1995). It constitutes a system of dextral strike-slip faults along which the cumulative right lateral shear reaches 6 mm a^{-1} (Authemayou *et al.* 2006; Walpersdorf *et al.* 2006).

Based on geodetic data (Walpersdorf *et al.* 2006) and inversion of earthquake focal mechanisms (Lacombe *et al.* 2006), the present-day shortening or compression directions are well constrained in the Northern and Central ZSFB. These directions are parallel and trend *c*. N25. This direction is slightly oblique to the *c*. N10° lithospheric convergence deduced from the Global Iran geodetic data (Vernant *et al.* 2004). This obliquity reflects a partitioning of oblique convergence in the western part of Fars Arc (Talebian & Jackson 2004; Authemayou *et al.* 2006).

Small-scale brittle deformation (Authemayou *et al.* 2006; Lacombe *et al.* 2006; Navabpour *et al.* 2007), calcite twinning (Lacombe *et al.* 2007) and AMS analyses (Bakhtari *et al.* 1998; Aubourg *et al.* 2004) provide a comprehensive pattern of Cenozoic palaeostress and strain data. The main trend of shortening or compression derived from these data is indicated in Figure 2b. It can be seen that a counter-clockwise rotation of the shortening direction is recorded in the Fars Arc from the Middle Miocene to the present. The palaeostress pattern will be discussed in the light of new AMS data.

Aubourg *et al.* (2008) proposed a first pattern of block rotations using palaeomagnetic data in the western Fars Arc. Both counter-clockwise and clockwise rotations have been reported mainly in the Agha-Jari Fm. (Fig. 3a). Although the dominant sense of rotation is clockwise, this first block rotation pattern does not support or rule out the various models of block rotations proposed by several researchers in the western Fars Arc (Bakhtari *et al.* 1998; Talebian & Jackson 2004; Molinaro *et al.* 2005; Authemayou *et al.* 2006; Lacombe *et al.* 2006; Navabpour *et al.* 2007).

New AMS results

Sampling

We sampled 10 sites in the limestone and marly limestone levels of the Palaeocene–Eocene carbonates of the Pabdeh Fm., four sites in the Miocene marly limestones of the Razk Fm., and 11 sites in the Mio-Pliocene clastic deposits of the Mishan and Agha-Jari Fms., from the western part of the Fars Arc, in the ZSFB (Fig. 3a). We cored rocks using a portable drilling machine and determined the geographical orientation using both magnetic compass and sun angles. Table 1 provides information about sampling, rock formation and bedding orientation. In Figure 3b, we indicate the sites in the stratigraphic column. We sampled one site in the Gurpi Fm., nine in the Padbeh Fm., four in the Razak Fm., two in the Mishan Fm. and nine in the Agha-Jari Fm. (Fig. 3). It should be noted that the four sites from the Mand anticline (8K–11K) were sampled in the Pliocene coastal Lahbari member (upper Agha-Jari Fm.). This may represent therefore the youngest deformation recorded by AMS. For palaeomagnetic and magnetic fabric investigations, we selected the finest-grained formations and sampled the paired limbs of anticlines or synclines. The Mio-Pliocene formations are contemporaneous with the folding events, especially the Agha-Jari Fm., where intraformational growth strata are commonly observed (Berberian & King 1981; Hessami *et al.* 2001; Homke *et al.* 2004; Sherkati & Letouzey 2004; Sherkati *et al.* 2005; Lacombe *et al.* 2006). All rocks sampled are weakly strained. Apart from small-scale brittle deformation (joints and faults), we never observed penetrative strain such as cleavage.

The Palaeocene sites are mainly located in the northern part of the ZSFB (north of 35°N latitude) on both sides of the Kazerun Fault (Fig. 3a). The Mio-Pliocene sites are in the southwestern part of the Fars Arc near the Kazerun, Karebass and Sabz-Pushan faults. Sites 1K, 2K, 5K (Palaeocene) and sites 6K and 7K (Mio-Pliocene) are close to the same Kazerun Fault segment. Sites 8K to 11K are in the Mand anticline, which is developed in front of the southernmost thrust termination of the Kazerun–Borazjan Fault (Authemayou *et al.* 2006; Sherkati *et al.* 2006; Oveisi *et al.* 2007). Sites 15K, 16K and 21K are situated in front of the southern termination of the Karebass Fault, where Permo-Triassic rocks are exhumed (Talebian & Jackson 2004). Sites 14K, 17K, 18K and 22K are along the Sabz-Pushan Fault. Only sites 19K and 20K are away from identified strike-slip faults.

AMS data

General behaviour. We measured the anisotropy of low-field magnetic susceptibility (AMS) of 327 standard oriented cores (*c*. 10 cm^3) using an Agico KLY-3S system. We processed the AMS data using standard tensorial Jelinek statistics (Jelinek 1978). Mean AMS data are compiled in Table 1. We plot in equal-area stereoplots the principal axes of the anisotropy ellipsoid ($K_1 \geq K_2 \geq K_3$) for each site, and the density diagrams of the K_1 and K_3 axes for two chronological groups of samples: the Mio-Pliocene and the Palaeocene rocks. We used three systems of coordinates: (1) the geographical coordinates (GC); (2) the stratigraphic coordinates (SC);

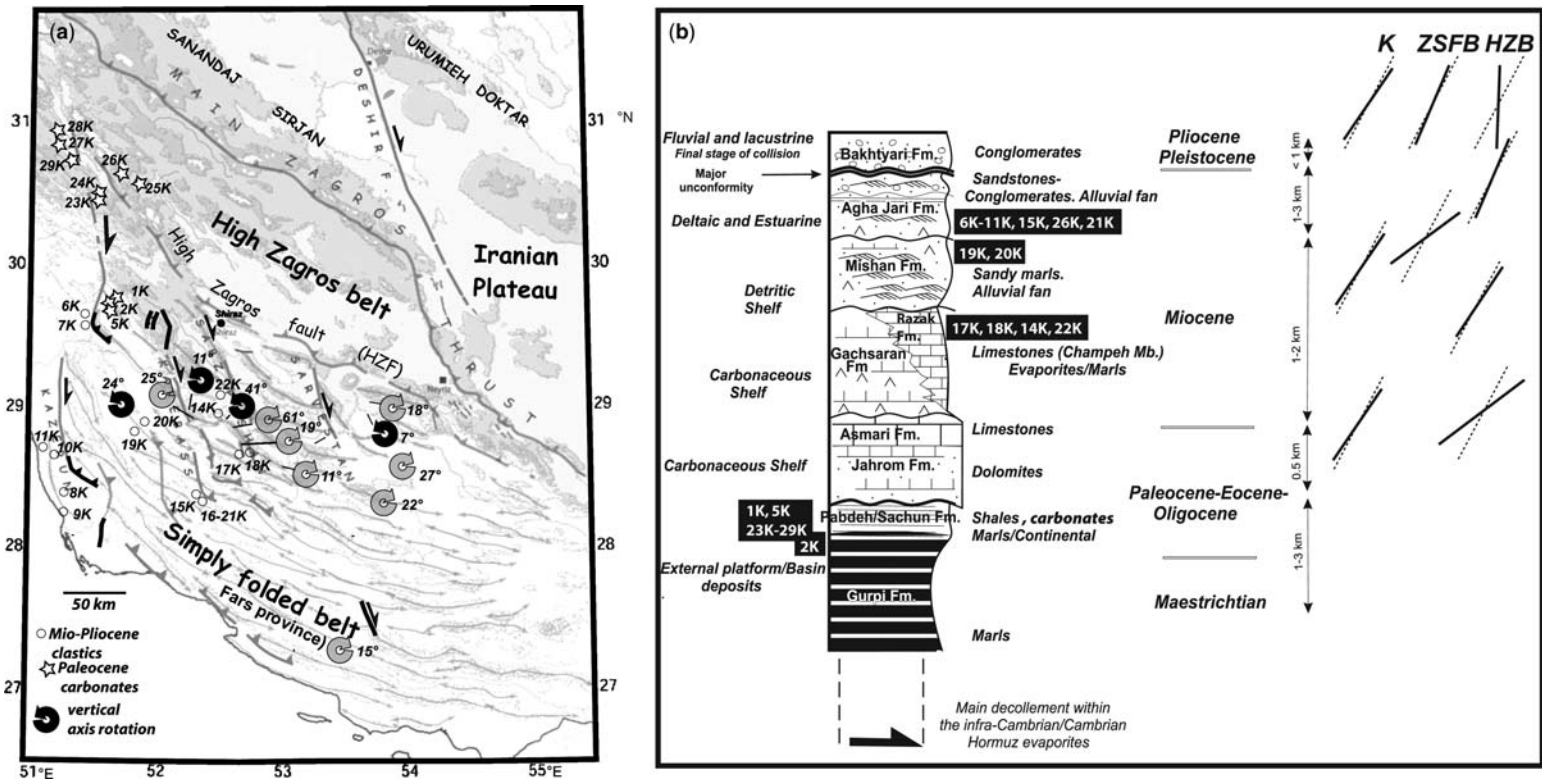

Fig. 3. (**a**) Location of the sites sampled. The vertical-axis rotation derived from palaeomagnetic data (Aubourg *et al.* 2008) is also indicated. (**b**) Stratigraphic column with location of sites. Also indicated is the shortening direction derived from brittle deformation analyses from the Kazerun Fault (K; Authemayou *et al.* 2006), Zagros Simply Fold Belt (ZSFB; Lacombe *et al.* 2006) and High Zagros Belt (HZB; Navabpour *et al.* 2007). Dashed lines represent the present-day shortening direction from GPS data.

Table 1. *Data for sites grouped by fold*

Site	Fold	Fm.	Age	Lithology	Latitude	Longitude	S_0	n	AMS Scalar data			GC				SC	
									K_m	P'	T	K_1	e_1/e_2	K_3	e_1/e_2	K_1	K_3
1 K	Chowgan	Padbeh	Paleocene	carbonates	29°48.10′	51°37.01′	290N25	16	26	1.014	0.64	338-20	27-9	222-14	9-9	161-0	253-76
2 K		Gurpi	Eocene	marls	29°47.65′	51°36.55′	192W12	12	39	1.018	0.62	311-5	11-9	78-82	10-8	131-6	323-84
5 K		Padbeh	Paleocene	carbonates	29°47.06′	51°35.27′	170W19	8	15	1.016	−0.17	226-40*	23-6	318-2*	12-7	232-24	138-9*
6 K	Rudak	Agha Jhari	Mio-Pliocene	red sandstones	29°37.68′	51°26.34′	256NW12	12	577	1.074	0.77	342-8	10-5	150-81	6-2	162-4	18-86
7 K		Agha Jhari	Mio-Pliocene	red sandstones	29°37.83′	51°26.96′	191W53	13	251	1.039	0.72	328-3	10-5	222-80	6-4	328-3	222-80
8 K	Mand	Lahbari	Mio-Pliocene	red sandstones	28°25.81′	51°17.30′	316E25	12	355	1.039	0.71	120-12	12-8	235-65	8-4	116-4	316-86
9 K		Lahbari	Mio-Pliocene	red sandstones	28°15.78′	51°16.84′	134W20	13	310	1.063	0.89	296-4	6-3	36-69	3-1	115-3	320-87
10 K		Lahbari	Mio-Pliocene	red sandstones	28°41.81′	51°12.20′	20E15	12	249	1.044	0.78	131-10	17-8	284-79	11-8	311-4	153-86
11 K		Lahbari	Mio-Pliocene	red sandstones	28°41.48′	51°07.36′	190W15	14	558	1.001	0.80	301-7	7-2	76-4	3-2	121-7	316-83
21 K	Daryau	Agha Jhari	Mio-Pliocene	red sandstones	28°18′46.6″	52°24′26.6‴	300NE34	15	670	1.074	0.44	121-4	5-2	216-55	5-2	119-2	240-86
15 K		Agha Jhari	Mio-Pliocene	red sandstones	28°20′19.6″	52°22′42.7‴	125SW40	15	324	1.024	−0.35	302-3	8-2	211-21	27-5	122-1	31-19
16 K		Agha Jhari	Mio-Pliocene	red sandstones	28°18′51.4″	52°24′25.4‴	295NE25	16	443	1.049	0.24	121-0	7-6	212-51	11-7	302-1	210-83
17 K	Qir	Razak	Miocene	red sandstones	28°51′19.0″	52°41′03.1‴	300NE41	12	93	1.030	0.71	115-11	10-3	216-46	4-2	110-2	315-88
18 K		Razak	Miocene	red sandstones	28°42′06.5″	52°42′32.6″	120SW46	11	72	1.034	0.73	136-10	15-3	36-41	5-3	319-2	71-86
19 K	Bushgan	Mishan	Miocene	marls	28°53′24.3″	51°49′26.9″	140SW15	14	586	1.087	0.59	151-7	5-2	35-76	4-2	152-0	277-89
20 K		Mishan	Miocene	marls	28°54′36.3″	51°52′14.4″	305NE15	12	539	1.121	0.80	143-3	7-2	244-76	3-2	142-7	324-84
14 K	Amirabad	Razak	Miocene	marls	28°57′49.6″	52°33′28.1‴	290NE52	13	91	1.027	0.71	288-3	6-5	195-50	6-3	290-2	47-86
22 K		Razak	Miocene	marls	29°03′49.7″	52°38′36.3‴	127SW57	14	59	1.030	0.62	286-37	4-3	39-28	3-2	266-2	72-88
23 K	Darihsk-East	Padbeh	Paleocene	carbonates	30°31′40.4″	51°32′32.7‴	130SW35	12	25	1.018	0.80	268-14	32-6	29-66	11-2	87-11	242-78
24 K		Padbeh	Paleocene	carbonates	30°32′11.7″	51°34′01.0‴	307N26	12	27	1.012	0.87	360-16	90-11	213-71	10-4	182-5	48-84
25 K	Vasag	Padbeh	Paleocene	carbonates	30°33′08.2″	51°40′18.2″	326NE75	17	14	1.015	0.73	148-7	17-5	241-25	5-5	140-4	30-79
26 K		Padbeh	Paleocene	carbonates	30°34′25.0″	51°39′09.3‴	326NE23	12	20	1.014	0.51	339-5	32-2	240-62	4-2	136-4	308-86
27 K	Darihsk-West	Padbeh	Paleocene	carbonates	30°43′17.2″	51°19′26.5‴	152SW40	14	10	1.016	0.62	167-13	90-6	62-52	24-5	353-1	239-88
28 K		Padbeh	Paleocene	carbonates	30°45′16.8″	51°19′25.5‴	265N15	13	48	1.025	0.66	301-5	7-3	192-75	3-2	121-4	271-86
29 K		Padbeh	Paleocene	carbonates	30°40′54.4″	51°24′45.5′	310N28	13	106	1.043	0.80	320-11	10-2	209-62	3-2	324-5	128-85

The formation (Fm.), stratigraphic age and lithology are indicated. Latitude and longitude locate the sampling sites. For bedding (S_0), numbers give strike (right-hand rule), dip direction, dip. n, number of samples measured. AMS scalar parameter. K_m, mean magnetic susceptibility, where $K_m = (K_1 + K_2 + K_3)/3$; 10^{-6} SI. P', corrected degree of anisotropy. $P = \exp\sqrt{2[(\eta_1 - \eta_m)^2 + (\eta_2 - \eta_m)^2 + (\eta_3 - \eta_m)^2]}$, where $\eta_i = \ln K_i$ and $\eta_m = (\eta_1 + \eta_2 + \eta_3)/3$. T, shape of AMS ellipsoid. $T = 2(\eta_1 - \eta_2)/(\eta_2 - \eta_3) - 1$. AMS direction K_1 and K_3 (declination/inclination) with their geographical coordinates (GC) and stratigraphic coordinates (SC). Confidence angles e_1/e_2 from Jelinek statistics (Jelinek 1978) are provided for geographical system of coordinates. For K_1, e_1 and e_2 refer to planes K_1–K_2 and K_1–K_3. For K_3, e_1 and e_2 refer to planes K_1–K_3 and K_2–K_3.

(3) the bedding strike coordinates (BSC). Rotating from GC to SC coordinates consists in untilting the AMS directions around the local bedding strike by an amount equal to the dip angle. In the BSC coordinates, a further vertical axis rotation is applied, so that all the local bedding strikes are rotated (clockwise or counter-clockwise) onto an arbitrary north reference direction, by the smallest angle between local strike and north (Aubourg *et al.* 2004). Quantitative information about AMS is provided by standard AMS parameters (Tarling & Hrouda 1993). K_m is the bulk magnetic susceptibility, P' is the degree of anisotropy, and T is the shape parameter. The definition and the mean values of these parameters are given in Table 1. K_m is a measure of magnetic grain concentration, including paramagnetic and ferromagnetic *sensu lato* minerals. P' is proportional to the degree of the magnetic grains' preferred orientation. It is dependent upon strain record, magnetic mineralogy and lithology (Rochette *et al.* 1992). When magnetic mineralogy and lithology are constant, P' is thus indicative of the degree of deformation. The shape factor T is also dependent upon strain, magnetic mineralogy and lithology. However, in thrust belts, the pattern of T from oblate ($+1$) to prolate (-1) is a good indication of increasing strain record (Averbuch *et al.* 1992; Parés *et al.* 1999; Aubourg *et al.* 2004; Robion *et al.* 2007).

To obtain an overall picture of the AMS data, we first show the density diagram of the AMS K_1 and K_3 axes in the three orientation systems (Fig. 4). In geographical coordinates, the K_3 axes are spread along a direction roughly perpendicular to the main fold axis trend. In the Mio-Pliocene formation, the main trend of K_3 axes is around *c*. N35°. In the Palaeocene formation, it is *c*. N45°. The magnetic lineations are subhorizontal. They are well grouped around *c*. N120° and *c*. N310° for the Mio-Pliocene and Palaeocene formations, respectively. In stratigraphic coordinates (Fig. 4), the K_3 are centred on the vertical axis in both the Mio-Pliocene and Palaeocene rocks, indicating that magnetic foliation is mostly parallel to bedding. The maximum density of magnetic lineations is at *c*. N120° and *c*. N130° for the Mio-Pliocene and Palaeocene rocks, respectively. It should be noted, however, that magnetic lineations are scattered around the horizontal plane, and in the NW and SE quadrants. For the Mio-Pliocene rocks, when the bedding strikes are transferred onto the north reference direction (BSC, Fig. 4a), the first maximum density of magnetic lineation is parallel to this direction, but a secondary maximum lies around N140°. In the Palaeocene formations, the magnetic lineations are much more scattered. The first maximum is observed at *c*. N35° (i.e. oblique to the bedding strike) but secondary maxima can also be seen around N10° and N150°.

The overall features of the magnetic fabric (i.e. magnetic foliation parallel to bedding and magnetic lineation parallel to the fold axis) indicate that magnetic fabric is essentially intermediate. The magnitude of the anisotropy parameters, P', as a function of the shape parameter, T, is also shown in Figure 4. The highest anisotropy factors are found in the clastic rocks, particularly in the Mishan black marls, and the lowest in the Palaeocene and Early Miocene carbonates. On average, the Mio-Pliocene clastic deposits and Palaeocene carbonates have values of $P' = 1.06 \pm 0.03$ and $P' = 1.02 \pm 0.01$, respectively. Bakhtari *et al.* (1998) observed the same difference of P' values. For a large majority of sites, the shape parameter is positive, indicating an oblate shape of AMS ellipsoid. On average, the Mio-Pliocene clastic deposits and Palaeocene carbonates have values of $T = 0.57 \pm 0.32$ and $T = 0.52 \pm 0.35$, respectively. Only sites 5K, 15K and 16K show negative values of T. At site 5K, the magnetic fabric, as we will see below, is inverse, which means that there is an exchange of AMS axes and an inverse trend of T value (Rochette *et al.* 1992). At sites 15K and 16K, we will see that there is a loss of bedding-related magnetic foliation as a result of a larger strain imprint, leading to a tectonic magnetic fabric. As a whole, the regional observations of magnetic fabric indicate therefore that the magnetic fabric is intermediate, with a magnetic lineation developing more or less parallel to the strike of the bedding.

Magnetic fabric at the fold scale. We now examine the magnetic fabric fold by fold (Fig. 5). At Mio-Pliocene sites, all magnetic foliations are parallel to bedding except at site 15K. The magnetic lineation is parallel to the strike of bedding and to the fold axis at folds 15K–16K–21K and 17K–18K. However, some magnetic lineations develop also oblique to the strike of bedding at folds 6K–7K, 8K–11K and 19K–20K and at site 22K. As a reference frame, we plot the shortening direction derived from geodetic data and inversion of earthquake focal mechanisms (N25°). We compare this direction with the AMS shortening direction (ASD). ASD is the strike of the vertical plane containing K_2 and K_3 after bedding correction. After bedding correction, we note that ASD, within the 95% uncertainty of mean magnetic lineation, is parallel to the present-day shortening direction at folds 8K–11K, 15K–16K–21K and 17K–18K. In contrast, ASD is rotated clockwise at folds 19K–20K and 6K–7K, and counter-clockwise at fold 14K–22K with respect to the present-day shortening direction. At Palaeocene sites, the magnetic foliation is mainly parallel to bedding. It should be noted, however, that the fabric is inverse at site 5K, where K_2 is close to the pole of bedding.

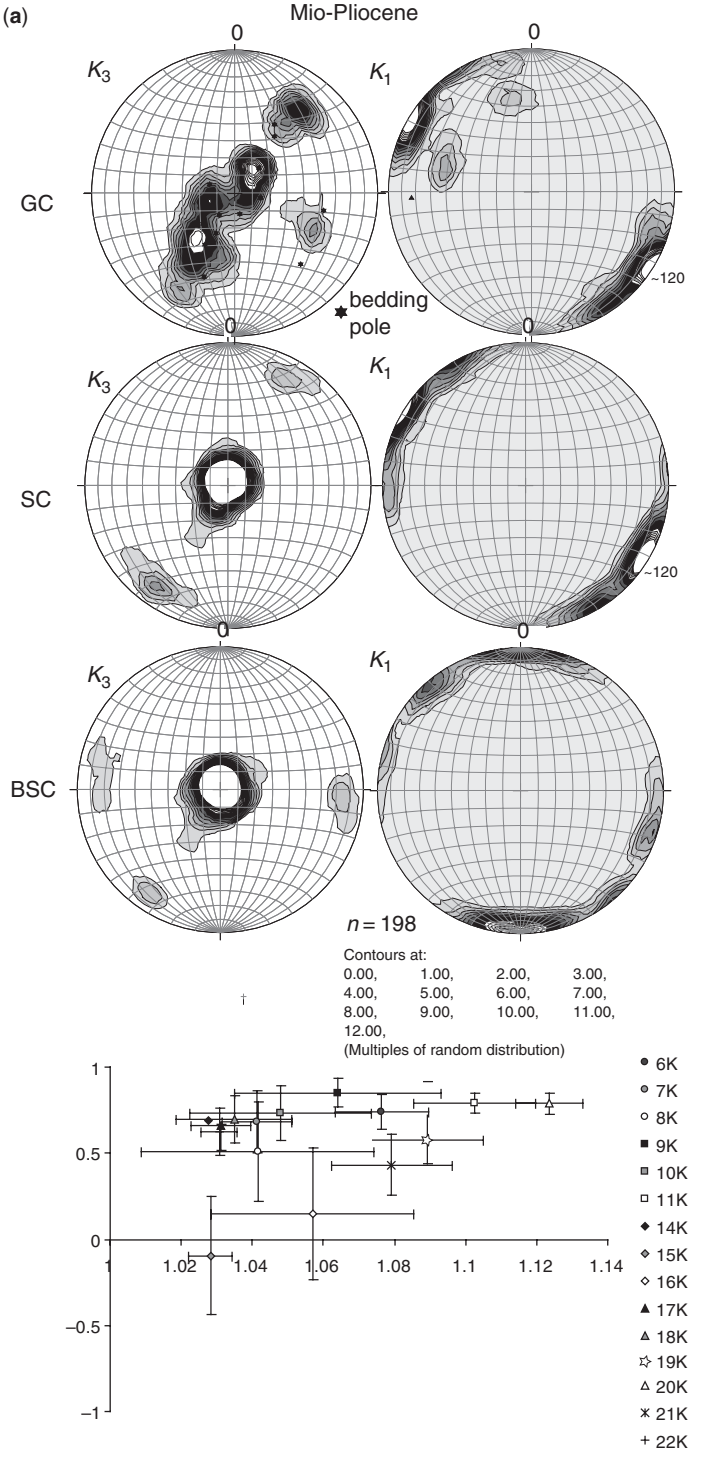

Fig. 4. AMS density diagrams produced using StereoNet. Stereographic projection in the lower hemisphere. GC, geographical coordinate; SC, stratigraphic coordinates; BSC, bedding strike coordinate. P' v. T and their standard deviation are shown (see Table 1 for definition of P' and T).

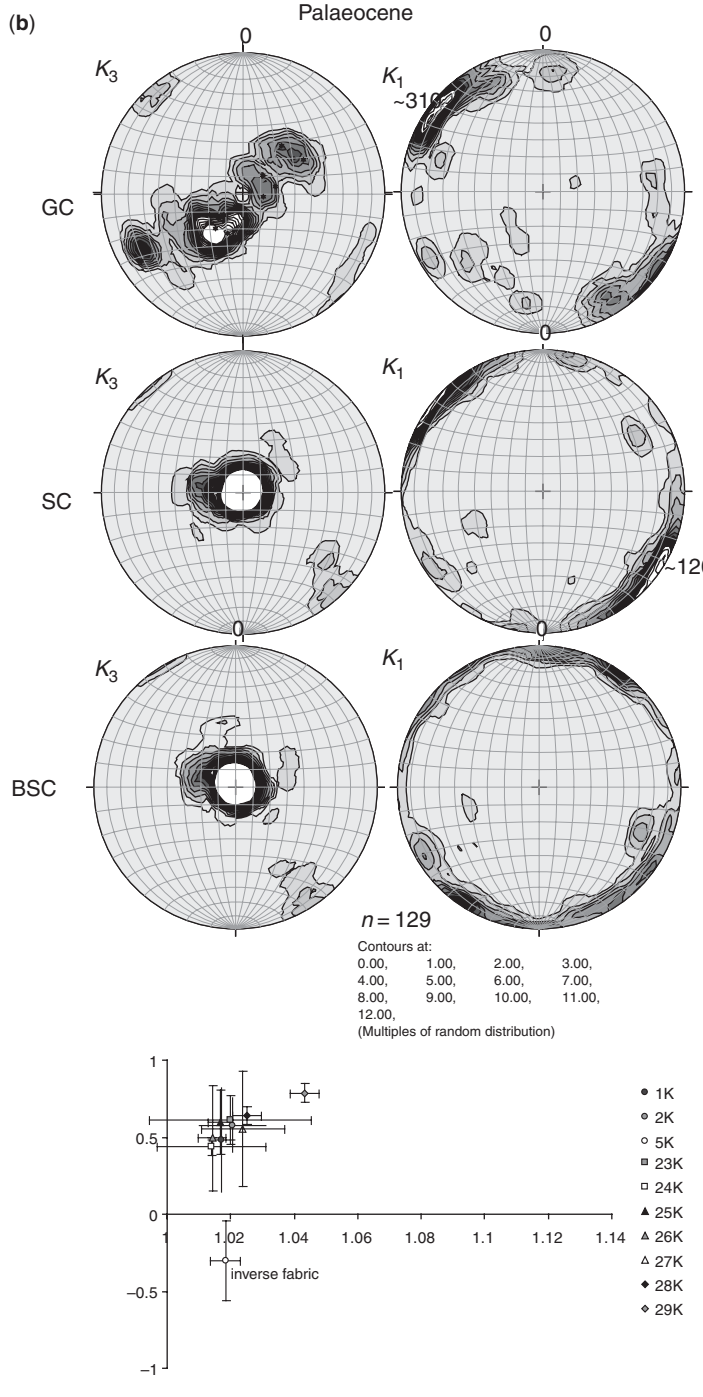
(b)
Palaeocene
0
K_3
K_1
~310
GC
SC
~120
BSC
$n = 129$
Contours at:
0.00, 1.00, 2.00, 3.00,
4.00, 5.00, 6.00, 7.00,
8.00, 9.00, 10.00, 11.00,
12.00,
(Multiples of random distribution)
1
0.5
0
−0.5
−1
1.02
1.04
1.06
1.08
1.1
1.12
1.14
inverse fabric
1K
2K
5K
23K
24K
25K
26K
27K
28K
29K

Fig. 4.

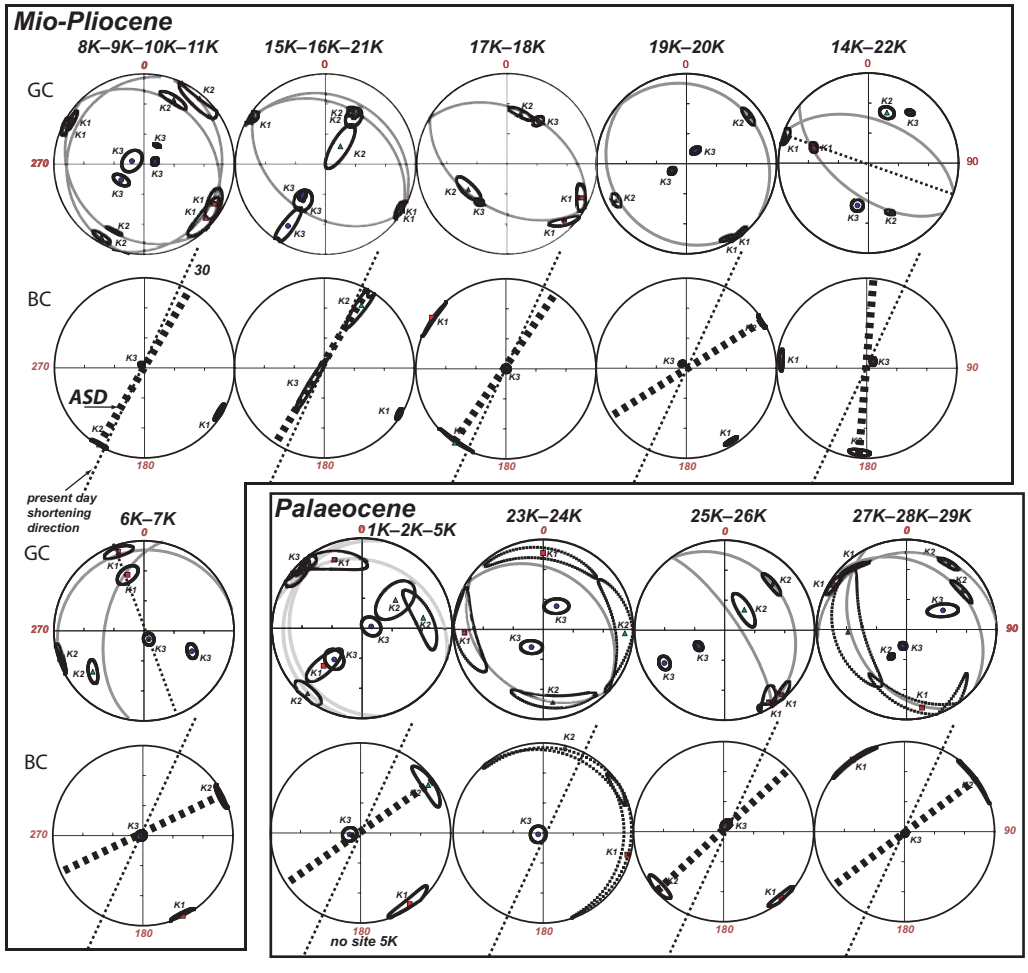

Fig. 5. AMS principal axes for the various folds, using the same conventions as in Figure 4. AMS K_1 (squares) K_2 (triangles) and K_3 (circles) are plotted with their confidence ellipse from the Jelinek's statistics (Jelinek 1978). ASD is the AMS shortening direction deduced from the K_2–K_3 vertical plane in stratigraphic coordinates. The present-day shortening direction is inferred from GPS (Walpersdorf *et al.* 2006).

Contrary to what observed in Plio-Miocene clastic deposits, the magnetic lineations are not as well defined in Palaeocene carbonates (see confidence angles in Table 1) because the magnetic fabric is dominantly of sedimentary origin. This is particularly true at fold 23K–24K, where the scatter of magnetic lineation is too large for any interpretation. However, the magnetic lineations are sufficiently accurate for interpretation in the other folds. ASDs are rotated clockwise with respect to the present-day shortening direction (Fig. 5).

We focus our attention to two specific folds: the Mand anticline, where oblique magnetic lineations are observed, and the syncline that develops in front of the Daryau anticline, where tectonic magnetic foliation is observed.

The Mand anticline provides a good example where the magnetic lineations are strongly oblique to the local strike of the bedding (Fig. 6). It is interesting to compare the Mand fold with its counterpart from the eastern Fars Arc: the Minab fold (Molinaro *et al.* 2004*a*; Smith *et al.* 2005). In both folds, AMS is measured from similar red sandstones. The location of these two folds is indicated in Figure 2c. The Landsat pictures of these folds with the major faults, AMS data, and ASD are shown in Figure 6. The Mand anticline, with its symmetrical *c*. 20° limbs, is a detachment fold that develops above the Cambrian Hormuz décollement level (Sherkati *et al.* 2006; Oveisi *et al.* 2007). The Minab anticline, with steep and asymmetrical limbs, is a fault propagation fold above a shallower

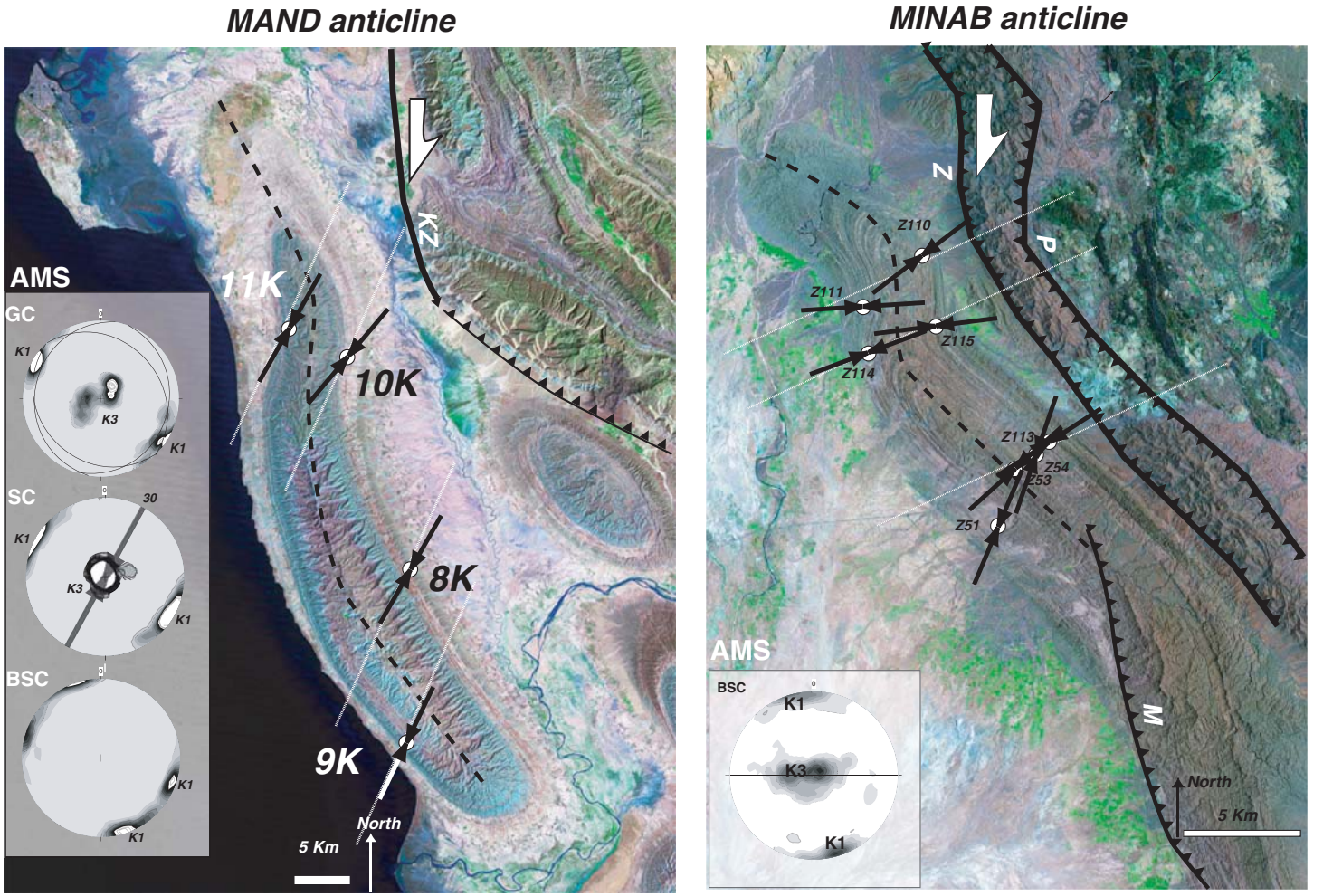

Fig. 6. Magnetic fabric in the Mand and Minab anticlines. (See Fig. 2b for location of these two folds). The Mand anticline is a detachment fold whereas the Minab anticline is a fault propagation fold. Black arrows, AMS shortening direction. It should be noted that the ASD is consistent in the Mand anticline but follows the strike of the bedding in the Minab anticline. White dashed line, present-day shortening direction inferred from GPS. KZ, Kazerun Fault; P, Palami Fault; Z, Zendan Fault; M, Minab Fault.

décollement level at 6 km depth (Molinaro *et al.* 2004*a*). In contrast to the Mand fold, where rocks are weakly strained, the deformation in the Minab anticline is much more pronounced (kink folds, jointing, spaced cleavage) (Aubourg *et al.* 2004; Molinaro *et al.* 2004*a*). The Mand and Minab folds show a distinct torsion in their northern part (Fig. 6). They are bounded to the NE by transpressive faults; the Kazerun Fault in the western Fars Arc (Authemayou *et al.* 2006), and the Zendan Fault in the eastern Zagros Makran Syntaxis (Regard *et al.* 2003). The Minab anticline is thrusted by the Zendan transpressive fault along its north-eastern margin (Regard *et al.* 2003).

The AMS pattern is different in the two folds. Whereas the magnetic foliation is parallel to the bedding in the Mand fold, the K_3 axes are slightly scattered along the strain direction in Minab fold (Fig. 6). Aubourg *et al.* (2004) interpreted this pattern as the record of a more intense strain compatible with field observation. The magnetic lineations form a distinguishable pattern in the two anticlines. In the Minab fold, the magnetic lineation follows the change of bedding strike, whereas the palaeomagnetic data demonstrate that the bedding strike torsion is primary (Smith *et al.* 2005). In contrast, the magnetic lineation in the Mand fold remains remarkably constant, despite a significant change (*c*. 50°) of bedding strike azimuth (Table 1). As a result, the magnetic lineations group better in bedding strike coordinates in the Minab fold, whereas magnetic lineations split into two groups in the Mand fold, indicating a moderate (*c*. 20°) and a strong (*c*. 70°) counter-clockwise rotation of the magnetic lineations with respect to the local fold axis strike (Fig. 6). In the Mand fold, the ASD is remarkably parallel to the present-day shortening direction. In the Minab fold, there is also a rather good consistency between ASD and the present-day shortening direction derived from geodetic data (Bayer *et al.* 2006).

Smith *et al.* (2005) proposed that the Minab fold developed above an inherited north–south-trending tectonic structure. Because the palaeostress pattern (AMS and brittle deformation) follows the strike of the bedding, this implies that stresses deviated near the north–south inherited structure, probably before the fault propagation fold development. In the Mand fold, the interpretation is different because there is no deviation of the palaeostress in relation to the strike of the bedding. Our data suggest that strain does not deviate because of inherited structure, if there is any. The obliquity of magnetic lineation with respect to the bedding strike strongly supports the Mand anticline being an oblique fold.

Throughout the western Fars Arc, the intermediate magnetic fabric as developed in the Mand anticline is the rule (Bakhtari *et al.* 1998; Aubourg *et al.* 2004). Nevertheless, a tectonic fabric is observed at sites 15K and 16K (Fig. 7d). These sites are located in a tight syncline, which developed in front of the Daryau anticline where overturned dips of the Guri Fm. are mapped in the core of the anticline (Fig. 7a). This is one of the rare places in ZSFB where overturned dips are identified. The Agha-Jari rocks are, however, weakly strained and only small-scale brittle deformation is observed (Fig. 7b). To better understand the situation of sites 15K and 16K–21K, we sketch the cross-section of the Daryau anticline (Fig. 7c) together with the three axes of the AMS ellipsoids for sites 15K and 16K (Fig. 7d). Some of the magnetic foliations are oblique to bedding and the K_3 axes are spread along a direction perpendicular to the fold trend. It is thus likely that sites 15K and 16K record a tectonic imprint related to the late thrusting stage of the Daryau anticline. Consistent with this, the ASD are parallel to the present-day shortening direction (Fig. 7a).

Interpretation of AMS results

Bakhtari *et al.* (1998) reported that about 55% of magnetic fabrics are intermediate with magnetic foliation parallel to bedding in the Fars Arc. Apart from sites 5K, 15K and 16K, all the sites studied in the present study display intermediate magnetic fabric (*c*. 92% of sites). In the western Fars Arc, we propose that the acquisition of magnetic fabric is mainly coeval with LPS. There are, however, some folds in which a tectonic magnetic foliation can develop simultaneously with folding and faulting near major active faults (Aubourg *et al.* 2004). One striking result of initial AMS studies in the Fars Arc is the recognition of magnetic lineation oblique to the fold axis. Bakhtari *et al.* (1998) observed at the scale of the western and central Fars Arc a *c*. 15° counter-clockwise obliquity between the magnetic lineation and the fold axis. Aubourg *et al.* (2004) reported both clock-wise and counter-clockwise obliquity larger than 30° at *c*. 40% of the sites in the eastern Fars Arc and Zagros–Makran Syntaxis. In the Mio-Pliocene rocks of the present study, the magnetic lineation K_1 is generally parallel to the fold axis trend, except in the Mand anticline (sites 8K–11K), in fold 6K–7K and at site 22K (Fig. 5), where K_1 is rotated counter-clockwise relative to the fold axis direction. At Palaeocene sites, it is difficult to determine an obliquity fold by fold, because the dispersion of the K_1 directions between the two opposite limbs of the folds is large. This is illustrated by the density diagram, where several maxima can be seen in bedding strike coordinates. We note, however, that the first maximum density

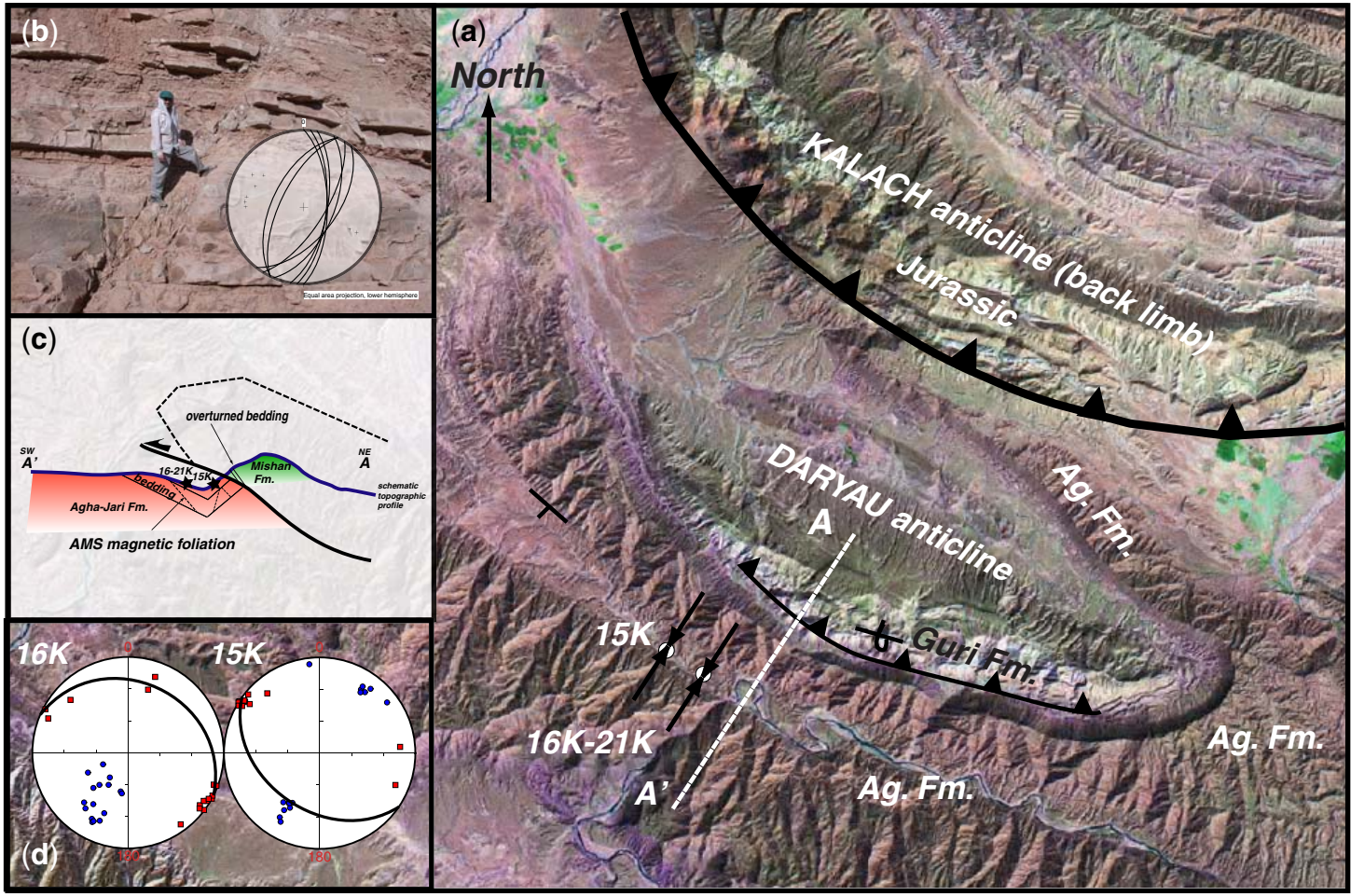

Fig. 7. Magnetic fabric in the footwall of the Daryau thrust. (**a**) Landsat picture. Sites 15K, 16K and 21K are sampled in Agha-Jari Fm (Ag. Fm). ASD is plotted (black arrows). A–A′, line of the cross-section shown in (**c**). (**b**) Photograph of Agha-Jari Fm. at site 16K. We see conjugate normal faults compatible with *c*. N120 extension. (**c**) Schematic cross-section. The attitude of magnetic foliation is sketched with respect to the bedding. (**d**) Magnetic fabric. Same convention as in Figure 5. Only axes K_1 (squares) and K_3 (circles) are plotted. Magnetic fabric is here tectonic, as shown by the incipient loss of bedding-parallel magnetic foliation at site 16K and the appearance of a tectonic magnetic foliation at site 15K.

of magnetic lineations is rotated clockwise with respect to the bedding strike.

Two mechanisms can explain the obliquity of the magnetic lineation with respect to the fold trend or bedding strike. A fold can develop obliquely above an inherited structure (Frizon de Lamotte *et al.* 1995; Smith *et al.* 2005). This is comparable with the 'forced' folds above blind thrusts as proposed in the ZSFB by several workers (Cosgrove & Ameen 2000; Sattarzadeh *et al.* 2000). Another plausible mechanism to explain the obliquity of magnetic lineation that the shortening direction changed between the onset of LPS and folding. We sketch in Figure 8 a two-step deformation phase: LPS followed by folding–faulting systems. We show in this system a blind fault, where forced folds can develop during folding. Between the two events, the shortening direction is rotated counter-clockwise. Our two-step model therefore combines the two mechanisms, oblique fold and rotation of the shortening direction. During LPS, we assume a regular imprint of a magnetic fabric as a result of stress (Fig. 8a). During folding and faulting (Fig. 8b), forced and frontal folds develop along and away from the fault, but in our hypothesis, the LPS-related magnetic fabric is preserved. In this model, we observe two kinds of oblique magnetic lineations. For the forced folds along the blind fault, we note a counter-clockwise obliquity of magnetic lineation with respect to the bedding (Fig. 8b). In contrast, for the frontal folds, we see a clockwise obliquity of magnetic lineation. According to this simple model, the *c.* 15° counter-clockwise obliquity evidenced both by Bakhtari *et al.* (1998) and the present dataset in the Agha-Jari Fm. may be explained either by forced folds above north–south-trending blind faults or by a clockwise rotation of the shortening direction through time, or a combination of both. It should be noted that Bakhtari *et al.* (1998) advocated a block rotation mechanism to explain the obliquity of magnetic lineations. Continuing in the frame of this model, we attempt to explain the oblique magnetic lineations observed at the Mand anticline. Rotation of the shortening direction is unlikely in the Mand anticline as the Lahbari Mb. is the youngest formation of Pliocene age sampled in this study. Thus, to account for the counter-clockwise obliquity of magnetic lineation with respect to the fold axis, the Mand anticline is probably a forced fold above a blind segment of a north–south-trending fault, which may be a possible southward extension of the Kazerun Fault as was suggested by Authemayou *et al.* (2006).

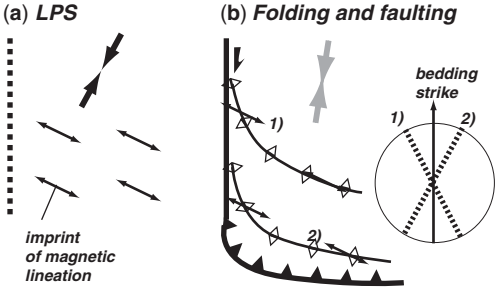

Fig. 8. Model of the development of oblique magnetic lineation. (**a**) Imprint of LPS by magnetic fabric. (**b**) Folding and faulting. Some folds develop oblique to the shortening direction (grey arrow). It should be noted that the shortening direction is rotated counter-clockwise with respect to LPS. Some magnetic lineations are oblique to the fold axis. As a result, magnetic lineations are not parallel to the bedding strike.

Discussion

Comparison of palaeostress markers

In the western Fars Arc, we have the opportunity to compare present-day shortening direction with palaeostress or palaeostrain data, derived from magnetic fabric, small-scale brittle deformation and calcite twinning analyses. These data are reported in Figure 9.

AMS data. The AMS shortening direction (ASD) derived from this study and Bakhtari *et al.* (1998) (Fig. 9a) provides essentially a picture of LPS, prior to folding. We see that the ASD pattern is rather homogeneous, apart from local deviations caused by uncertainties of magnetic lineations (see Table 1) or tectonic complication such as block rotation (see Fig. 3a). From the western to central Fars Arc, ASD swings from a NE–SW to a north–south direction as previously observed by Bakhtari *et al.* (1998). For the new set of AMS data confined to the western Fars Arc, there is an overall good agreement between ASD and present-day shortening direction in the Mio-Pliocene formations to the south, and a systematic *c.* 10° clockwise deviation for the Palaeocene formations (Figs 5 & 9a). When combining AMS data from the present study and from Bakhtari *et al.* (1998) restricted to the western Fars Arc, we obtain an LPS direction at N47° ± 13° (eight sites) for the Palaeocene formations and N38° ± 32° (31 sites) for the Mio-Pliocene formations.

Fault slip data. We report the palaeostress σ_1 trends (Fig. 9b) resulting from the inversion of the small-scale brittle deformation from two studies (Authemayou *et al.* 2006; Lacombe *et al.* 2006). As noted in the introduction, small-scale brittle deformation can record all steps of deformation during the formation of a thrust belt (Fig. 1). The

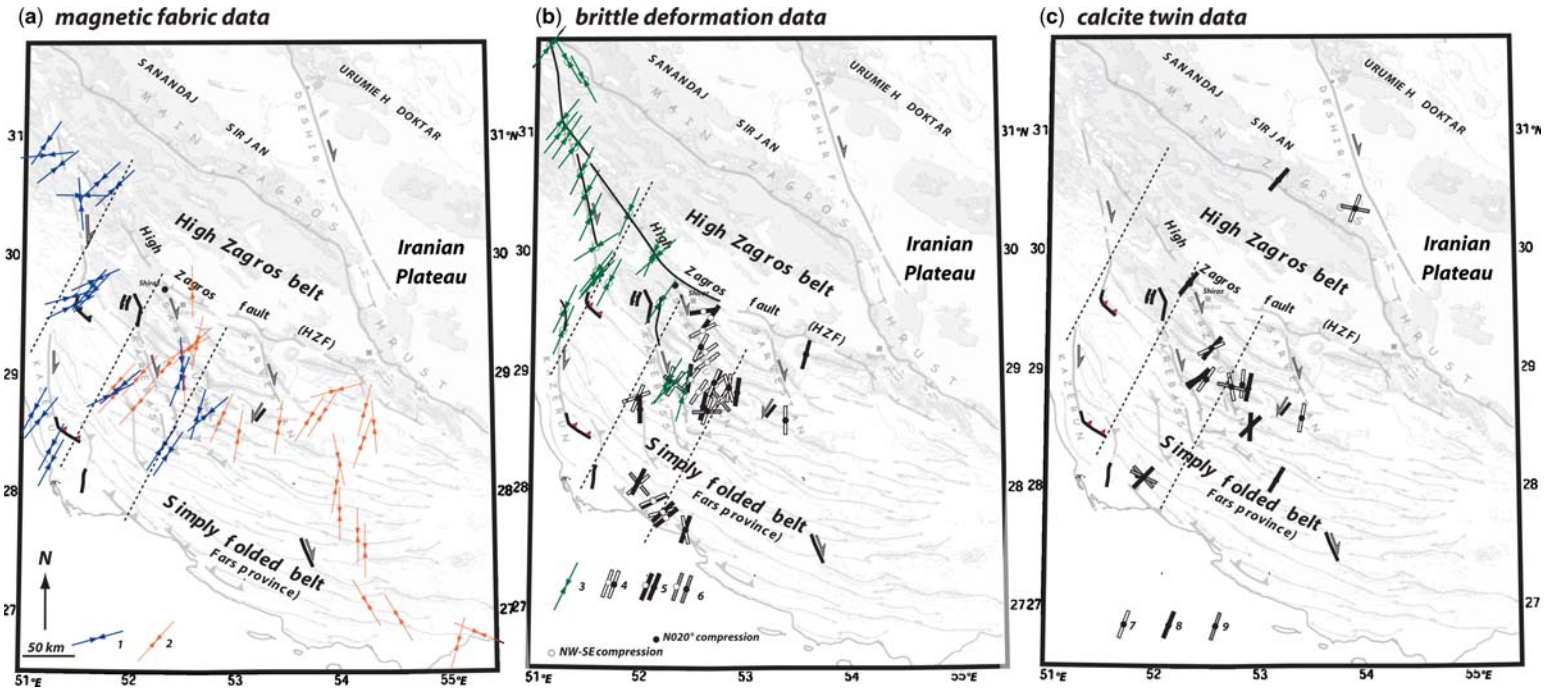

Fig. 9. Palaeostress map. (**a**) AMS shortening direction. 1, From this study; 2, from Bakhtari *et al.* (1998). (**b**) Brittle deformation data. 3, Compressional trends from Authemayou *et al.* (2006); 4–6, compressional or extensional trends from Lacombe *et al.* (2006) (4, compressional trend, strike-slip regime; 5, compressional trend, compressional regime; 6, extensional trend, extensional regime). (**c**) Calcite twin data (Lacombe *et al.* 2007). 7, Compressional trend, strike-slip regime; 8, compressional trend, compressional regime; 9, extensional trend, extensional regime. Dashed lines represent the present-day shortening direction inferred from earthquake focal mechanisms (Lacombe *et al.* 2006).

identification and separation of successive generations of faults and related stress regimes is based on both mechanical incompatibility between fault slips (single misfits of fault slips with the computed stress tensors) and relative chronology observations (e.g. superimposed striations on fault surfaces, crosscutting relationships between faults). To establish a time distribution of tectonic regimes, dating of the brittle structures also requires stratigraphic information about the age of the deformed units and/or evidence of syndepositional tectonism. Particular attention was also paid to horizontal-axis rotations of rock masses as a result of folding. During folding, several cases deserve consideration, because faults may have formed before, during or after folding. For instance, pre-folding strike-slip faults, a common feature in the SFB, can be unambiguously identified by the attitude of the striations, which always lie within the bedding regardless of the strata attitude, and thus have to be interpreted in their back-rotated attitude. Following Anderson (1951), it is assumed that away from major fault zones one of the three principal stress axes of a tensor is generally vertical. If a fault set formed before folding and was secondarily tilted with the bedding, the tensor calculated on this set does not display a vertical axis. Instead, one of the stress axes is generally found to be perpendicular to bedding, whereas the two others lie within the bedding plane. In such a case, the fault system is interpreted after back tilting to its initial position. Within a heterogeneous fault population this geometrical reasoning allows separation of data subsets based on their age relative to fold development (Fig. 10). In the case of the very simple geometry and cylindrical character of folds in the Zagros

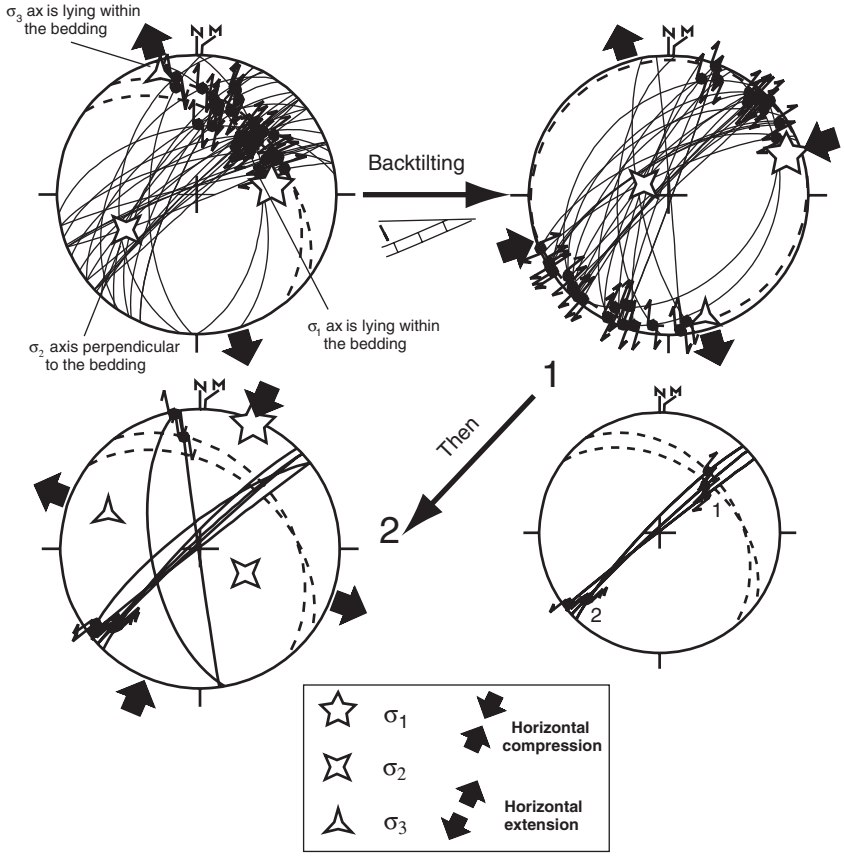

Fig. 10. Example of chronological relationships between faulting related to ENE–WSW compression and faulting related to N020° compression in limestones from the Champeh Member of the Gachsaran Fm. Stereodiagrams in the left part of the figure show striated microfaults in their current attitude (tilted strata), in contrast to the upper right diagram, in which faults related to ENE–WSW compression have been backtilted with bedding. The first strike-slip system predates folding as revealed by the attitude of principal stress axes and striations with respect to bedding; the N020° compression reactivates some faults consistent with the former stress regime and post-dates folding.

SFB, this criterion is of primary importance for establishing a relative chronology. This criterion is further combined with dating of fold development using unconformities and growth strata within synorogenic deposits. The chronology inferred in this way is usually confirmed by identification of superimposed striations on reactivated fault surfaces where observable; it therefore reliably reflects the local succession of faulting events and related stress regimes.

We discuss first the palaeostress pattern in the area of the Karebass and Sabz Pushan faults (Lacombe *et al.* 2006) and then the palaeostress pattern along the Kazerun Fault (Authemayou *et al.* 2006).

For the Karebass and Sabz Pushan faults, the first faulting event is marked by reverse and strike-slip faults and is related to a compressional trend striking NE–SW to ENE–WSW on average. When bed tilting is sufficiently steep to prevent uncertainties, it can be unambiguously identified as having occurred mainly before folding, but also sometimes during and after folding. Although these observations were not always made together at all sites, this compression is clearly associated with the main folding phase at the regional scale.

A more recent faulting event related to a N20° compression has been distinguished from the previous NE–SW compression. At sites where both compressions have been recognized, superimposed striations on fault surfaces and considerations of fault v. bedding attitudes suggest that the N20° compression-related faulting episode postdates that related to the NE–SW compression. We show an example of a superimposed record of pre-tilting and post-tilting deformation (Fig. 10). In this example, some NE–SW-trending strike-slip faults show two striations, the horizontal ones indicating left-lateral motion cutting the NE-dipping ones consistent with right-lateral motion. Additionally, the latter lie within the bedding as the σ_1 and σ_3 axes of the computed stress tensor, whereas the σ_2 axis is perpendicular to bedding. This means that faulting related to the NE–SW compression occurred first, mainly before local folding, and must be interpreted as the earliest event. It predates fault development related to the N20° compression, which clearly occurred after folding. At most sites, faulting related to the N20° compression postdates folding. However, folding may have continued and probably ended during this faulting event, at least locally.

For the Kazerun Fault, inversions of the fault slip data indicate a strike-slip regime with a N35–40°E-trending σ_1 with a mean value of N36° ± 15°. Stress tensors determined within Mesozoic rocks are consistent within 10° with the stress tensors deduced from inversion of data collected within Pliocene to Quaternary sediment (N27°). Consequently, no significant change of σ_1 trend has been observed along the Kazerun system. This constancy could be attributed to the reorientation and partitioning mechanisms near this major structural boundary.

Calcite twin data. We plot the main compressional trends σ_1 resulting from the inversion of calcite twinning data collected in both fold-related veins and host rocks with ages ranging from Late Cretaceous to Middle Miocene (Lacombe *et al.* 2007) (Fig. 9c). The relationship between the palaeostress axes and bedding indicates that calcite twinning mainly recorded the late stage of folding (fold tightening) rather than the LPS. As is generally the case for fault slip data and for earthquake focal mechanisms (Lacombe *et al.* 2006), the stress regime is either truly compressional (vertical σ_3 axis) or strike-slip (vertical σ_2 axis), without any obvious regional variation and chronology in the results (except close to the Kazerun Fault). It should be noted that some samples also reveal a component of fold-parallel extension. On average, σ_1 trends N25 ± 15° (Lacombe *et al.* 2007, on 16 analyses). We observe, however, some departures from the N25 trend. These results are in good agreement with the post-folding palaeostress data of Lacombe *et al.* (2006). In addition, the estimated pre-folding (although few) and post-folding differential stress magnitudes obtained from the twinning analysis are low and, to a first approximation, they are constant across the Zagros Simply Folded Belt. This led Lacombe *et al.* (2007) to propose that most of the folds in the ZSFB formed under low differential stresses and resulted from buckling of the detached Zagros cover, as fault-related folding would be expected to have occurred under higher differential stresses owing to friction on the ramps. The overall constant wavelength of folds, their nearly coeval development and hence the first-order absence of clear propagation of deformation across the SFB, and their rapid growth rates also support buckling of the cover (Mouthereau *et al.* 2006). This is in line with the value of the AMS shape parameter *T*, which is generally larger than 0.5 (see Table), indicating for a weak input of strain and limited internal deformation. Therefore both independent calcite twinning and AMS approaches support the hypothesis that most folds in the ZSFB are mainly detachment folds (Falcon 1961; Molinaro *et al.* 2003; Sherkati *et al.* 2005; Mouthereau *et al.* 2006).

Integrating palaeostress data

Several workers agree on a two-stage model of formation of the Zagros thrust-and-fold belt since the Miocene (Molinaro *et al.* 2004, 2005; Sherkati *et al.* 2005, 2006; Mouthereau *et al.* 2007*a*, *b*).

The first stage is a wide detachment-folding phase (or buckling phase) in both the High Zagros Belt and the Zagros Simply Fold Belt (Mouthereau *et al.* 2007*a*), as a result of the decoupling of the sedimentary cover above the 1 km thick Eo-Cambrian Hormuz Salt Fm. The precise age of this tectonic phase is still debated. It is considered to start in the Early Miocene and finish at the end of Middle Miocene in the HZB, based on the observation of unconformities (Navabpour *et al.* 2007). In the ZSFB, the buckling phase occurred during the Late Miocene to Pliocene, based on the observation of growth strata in the Upper Agha-Jari Fm. (Homke *et al.* 2004; Sherkati *et al.* 2005; Lacombe *et al.* 2006). The second folding stage occurred mainly in the ZSFB after the deposition of the Bakhtyari Fm. It consists mostly of fold reactivation and generalized blind basement faulting. This tectonic phase is still active at present throughtout the ZSFB, although the Quaternary deformation is essentially localized in the frontal folds (Oveisi *et al.* 2007).

Although the above-mentioned studies agree on the broad lines of the folding history and with the major present-day role of the basement, it must be mentioned that there is no general agreement on the timing of these two tectonic phases, nor on the time when the basement was first involved in the Zagros deformation. In the present study, we attempt to combine all the palaeostress and palaeostrain data, including those of Navabpour et al. (2007) for the HZB, in a comprehensive scheme of a two-stage formation of the High Zagros Belt and the Zagros Simply Folded Belt (Fig. 11).

During the buckling stage in the HZB, our data support the idea that rocks older than the Mishan Fm. and Agha-Jari Fm. of the ZSFB experienced both LPS and faulting. This is the first step of our model in Figure 11a. We plot Early to Middle Miocene data of Navabpour *et al.* (2007), pre-folding fault slip data from Lacombe *et al.* (2006), and Palaeocene AMS data (this study) for this first buckling step. It should be noted that pre-folding fault slip data are here interpreted as older than in the previous interpretation by Lacombe *et al.* (2006). It can be seen that there is a good agreement between all the data, indicating a main NE shortening direction. When the buckling stage occurred in the ZSFB during the Late Miocene (Fig. 11b), the AMS data from the Agha-Jari Fm., calcite twin palaeostress data (2007), late Miocene to Early Pliocene palaeostress data from the HZB (Navabpour *et al.* 2007), and syn- to post-folding palaeostress data from the ZSFB (Lacombe *et al.* 2006) are all consistent with a shortening direction between

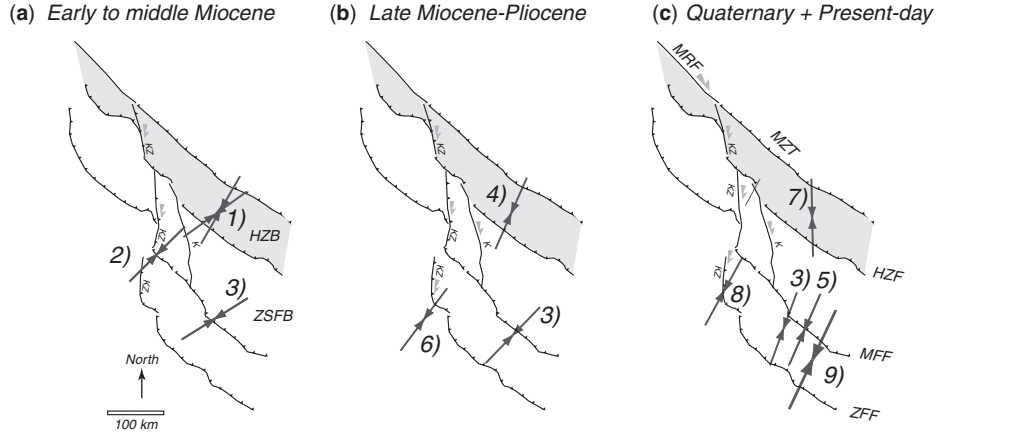

Fig. 11. Tectonic scenario of folding in the Zagros belt and related palaeostress data. (**a**) Detachment folding in the HZB and coeval LPS–faulting in the ZSFB; (**b**) detachment folding in the ZSFB; (**c**) late fold rejuvenation in the ZSFB; only faulting occurred in the HZB. KZ, Kazerun Fault; K, Karebas Fault; HZF, High Zagros Fault; MFF, Mountain Front Fault; ZFF, Zagros Front Fault; MZT, Main Zagros Thrust; MRF, Main Recent Fault.

N25 and N45, although a counter-clockwise rotation of shortening is locally suspected using fault slip data (Lacombe *et al.* 2006). For the second folding phase, which consists mainly of fold rejuvenation, we plot (Fig. 11c) the recent palaeostress recorded by Quaternary sediments along the Kazerun Fault (Authemayou *et al.* 2006), Late Pliocene to recent fault slip data in the HZB (Navabpour *et al.* 2007), inversion of focal mechanisms of earthquakes from the western Fars Arc (Lacombe *et al.* 2006) and the GPS-derived shortening trend (Walpersdorf *et al.* 2006). All these data reveal that the shortening direction remains more or less at N20–N30 in the ZSFB, but instead trends north–south in the HZB.

Our model therefore shows that it is possible to fit the palaeostress data from the HZB and the ZSFB within the uncertainties of the dataset and the history of deformation. A counter-clockwise rotation of at least 10° of the shortening direction between the first stage of folding in the HZB (buckling) and the second stage of folding in the ZSFB (fold rejuvenation) is likely. This rotation is possibly due to far-field geodynamic constraints as discussed by Navabpour *et al.* (2007), or to clockwise block rotations close to the set of right-lateral strike-slip faults bounding the Fars Arc to the west as initially stated by Bahktari *et al.* (1998) and developed by Lacombe *et al.* (2006). Whatever its origin, the counter-clockwise rotation of the shortening direction has consequences for the palaeostress regime during faulting, especially along these major strike-slip faults. Although this tendency is not clear throughout the ZSFB, fault slip data collected from the HZB and along the Kazerun Fault support a temporal evolution from reverse to strike-slip regimes (Authemayou *et al.* 2006; Navabpour *et al.* 2007). This is consistent with a counter-clockwise rotation of the shortening direction, and this may explain how an initial thrust trending NW–SE during the first stage of folding in the HZB evolved into a transpressive fault during the second folding stage in the ZSFB and in the faulting stage in the HZB.

Conclusion

To recover the imprint of palaeostress and -strain during the development of the Zagros Simply Folded Belt, we have performed an integrated study of palaeostress data obtained by different techniques, including magnetic fabric, fault slip and calcite twinning data. The magnetic fabric from Palaeocene carbonates and Mio-Pliocene clastic deposits retains the record of the layer-parallel shortening (LPS) that occurred prior to folding. We propose that the Palaeocene carbonates record a N47° ± 13° LPS during early to middle Miocene detachment folding in the High Zagros Belt. Before or during later (late Miocene–Pliocene) detachment folding in the ZSFB, the Mio-Pliocene clastic deposits recorded the N38° ± 32° LPS. Fault slip and calcite twinning data recorded a two-stage folding in the ZSFB: first the detachment folds and then a reactivation of folds. All the techniques suggest a counter-clockwise rotation of the shortening direction from NE to N20° between the onset of the detachment-fold phase of the HZB and the late stage of the detachment-fold phase of the ZSFB.

This work was funded by a DYETI programme led by D. Hatzfeld. The Geological Survey of Iran, thanks to Dr M. R. Ghassemi, provided invaluable help in logistics and science. We have benefited from constructive discussion with members of the DYETI and MEBE groups. D. Frizon de Lamotte is particularly thanked for reviewing the initial manuscript.

References

ANDERSON, E. M. 1951. *The Dynamics of Faulting*. Oliver & Boyd, White Plains, NY.

ANGELIER, J. 1990. Inversion of field data in fault tectonics to obtain the regional stress—III. A new rapid direct inversion method by analytical means. *Geophysical Journal International*, **103**, 363–376.

AUBOURG, C., FRIZON DE LAMOTTE, D., POISSON, A. & MERCIER, E. 1997. Magnetic fabrics and oblique ramp-related folding. A case study from the Western Taurus (Turkey). *Journal of Structural Geology*, **19**, 1111–1120.

AUBOURG, C., SMITH, B. *ET AL.* 2004. Post-Miocene shortening pictured by magnetic fabric across the Zagros–Makran syntaxis. *In*: SUSSMAN, A. B. (ed.) *Orogenic Curvature: Integrating Palaeomagnetic and Structural Analyses*. Geological Society of America, Special Papers, **383**, 17–40.

AUBOURG, C., SMITH, B., BAKHTARI, H., GUYA, N. & ESHRAGHI, A. R. 2008. Tertiary block rotations in the Fars Arc (Zagros, Iran). *Geophysical Journal International*, **173**, 659–673.

AUTHEMAYOU, C., CHARDON, D., BELLIER, O., MALEKZADEH, Z., SHABANIAN, E. & ABBASSI, M. R. 2006. Late Cenozoic partitioning of oblique plate convergence in the Zagros fold-and-thrust belt (Iran). *Tectonics*, **25**, TC3002.

AVERBUCH, O., FRIZON DE LAMOTTE, D. & KISSEL, C. 1992. Magnetic fabric as a structural indicator of the deformation path within a fold–thrust structure: a test case from the Corbières (NE Pyrenees, France). *Journal of Structural Geology*, **14**, 461–474.

BAKHTARI, H., FRIZON DE LAMOTTE, D., AUBOURG, C. & HASSANZADEH, J. 1998. Magnetic fabric of Tertiary sandstones from the Arc of Fars (Eastern Zagros, Iran). *Tectonophysics*, **284**, 299–316.

BAYER, R., CHERY, J. *ET AL.* 2006. Active deformation in Zagros–Makran transition zone inferred from GPS measurements. *Geophysical Journal International*, **165**, 373–381.

BERBERIAN, M. 1995. Master 'blind' thrust faults hidden under the Zagros folds: active basement tectonics and surface morphotectonics. *Tectonophysics*, **241**, 193–224.

BERBERIAN, M. & KING, G. C. P. 1981. Towards a paleogeography and tectonic evolution of Iran. *Canadian Journal of Earth Sciences*, **18**, 210–265.

BLANC, E. J.-P., ALLEN, M. B., INGER, S. & HASSANI, H. 2003. Structural styles in the Zagros Simply Folded Zone, Iran. *Journal of the Geological Society, London*, **160**, 401–412.

BORRADAILE, G. J. 1987. Anisotropy of magnetic susceptibility: rock composition versus strain. *Tectonophysics*, **138**, 327–329.

BURKHARD, M. 1993. Calcite twins, their geometry, appearance and significance as stress–strain markers and indicators of tectonic regime: a review. *Journal of Structural Geology*, **15**, 351–368.

COSGROVE, J. W. & AMEEN, M. S. 2000. A comparison of the geometry, spatial organisation and fracture patterns associated with forced folds and buckle folds. *In*: COSGROVE, J. W. & AMEEN, M. S. (eds) *Forced Folds and Fractures*. Geological Society London, Special Publications, **169**, 7–21.

CRADDOCK, J. P. & VAN DER PLUIJM, B. 1999. Sevier–Laramide deformation of the continental interior from calcite twinning analysis, west–central North America. *Tectonophysics*, **305**, 275–286.

ETCHECOPAR, A. 1984. *Etude des états de contraintes en techonique cassante et simulation des déformations plastiques*, PhD thesis, Montpellier University, France, 270.

FALCON, N. L. 1961. Major earth-flexuring in the Zagros mountains of south-west Iran. *Quarterly Journal of the Geological Society*, **117**, 367–376.

FRIZON DE LAMOTTE, D., GUEZOU, J.-C. & AVERBUCH, O. 1995. Distinguishing lateral folds in thrust-systems; examples from Corbières (SW France) and Betic Cordillieras (SE Spain). *Journal of Structural Geology*, **17**, 233–244.

FRIZON DE LAMOTTE, D., SOUQUE, C., GRELAUD, S. & ROBION, P. 2002. Early record of tectonic magnetic fabric during inversion of a sedimentary basin. Short review and examples from the Corbières transfer zone (France). *Bulletin de la Société Géologique de France*, **173**, 461–469.

GRAHAM, J. W. 1966. Significance of magnetic anisotropy in Appalachian sedimentary rocks. *In*: STEINHART, J. S. & SMITH, T. J. (eds) *The Earth Beneath the Continents*. American Geophysical Union, Geophysical Monograph, **10**, 627–648.

HAMILTON, T. D., BORRADAILE, G. J. & LAGROIX, F. 2004. Sub-fabric identification by standardization of AMS: an example of inferred neotectonic structures from Cyprus. *In*: MARTIN-HERNANDEZ, F., LUNEBURG, C. M., AUBOURG, C. & JACKSON, M. (eds) *Magnetic Fabric: Methods and Applications*. Geological Society, London, Special Publications, **238**, 527–540.

HARRIS, J. H. & VAN DER PLUIJM, B. A. 1998. Relative timing of calcite twinning strain and fold–thrust belt development: Hudson Valley fold–thrust belt. New York, USA. *Journal of Structural Geology*, **20**, 21–31.

HESSAMI, K., KOYI, H. A., TALBOT, C. J., TABASI, H. & SHABANIAN, E. 2001. Progressive unconformities within an evolving foreland fold–thrust belt, Zagros Mountains. *Journal of the Geological Society, London*, **158**, 969–981.

HESSAMI, K., NILFOROUSHAN, F. & TALBOT, C. J. 2006. Active deformation within the Zagros Mountains deduced from GPS measurements. *Journal of the Geological Society, London*, **163**, 143–148.

HIRT, A. M., EVANS, K. F. & ENGALDER, T. 1995. Correlation between magnetic anisotropy and fabric for Devonian shales on the Appalachian plateau. *Tectonophysics*, **247**, 121–132.

HOMKE, S., VERGES, J., GARCES, M., EMAMI, H. & KARPUZ, R. 2004. Magnetostratigraphy of Miocene–Pliocene Zagros foreland deposits in the front of the Push-e Kush Arc (Lurestan Province, Iran). *Earth and Planetary Science Letters*, **225**, 397–410.

HROUDA, F. 1982. Magnetic anisotropy of rocks and its application in geology and geophysics. *Geophysical Surveys*, **5**, 37–82.

HROUDA, F., PROS, Z. & WOHLGEMUTH, J. 1993. Development of magnetic and elastic anisotropies in slates during progressive deformation. *Physics of the Earth and Planetary Interiors*, **77**, 251–265.

JELINEK, V. 1978. Statistical processing of anisotropy of magnetic susceptibility mesured on group of specimen. *Studia Geophysica et Geodaetica*, **22**, 50–62.

JELINEK, V. 1981. Characterization of the magnetic fabric of the rocks. *Tectonophysics*, **79**, 63–67.

KANAMATSU, T., HERRERO-BERVERA, E. & ASAHIKO, T. 2001. Magnetic fabric of soft-sediment folded strata within a neogene accretionary complex, the Miura group, Central Japan. *Earth and Planetary Science Letters*, **187**, 333–343.

KISSEL, C., BARRIER, E., LAJ, C. & LEI, T.-Q. 1986. Magnetic fabric in 'undeformed' marine clays from compressional zones. *Tectonics*, **5**, 769–781.

LACOMBE, O. 2001. Palaeostress magnitudes associated with development of mountain belts: Insights from tectonic analyses of calcite twins in the Taiwan Foothills. *Tectonics*, **20**, 834–849.

LACOMBE, O. 2007. Comparison of palaeostress magnitudes from calcite twins with contemporary stress magnitudes and frictional sliding criteria in the continental crust: Mechanical implications. *Journal of Structural Geology*, **29**, 86–99.

LACOMBE, O., MOUTHEREAU, F., KARGAR, S. & MEYER, B. 2006. Late Cenozoic and modern stress fields in the western Fars (Iran): implications for the tectonic and kinematic evolution of central Zagros. *Tectonics*, **25**, TC1003.

LACOMBE, O., AMROUCH, K., MOUTHEREAU, F. & DISSEZ, L. 2007. Calcite twinning constraints on late Neogene stress patterns and deformation mechanisms in the active Zagros collision belt. *Geology*, **35**, 263–266.

MASSON, F., CHERY, J., HATZFELD, D., MARTINOD, J., VERNANT, P., TAVAKOLI, F. & GHAFORY-ASHTIANI, M. 2005. Seismic versus aseismic deformation in Iran inferred from earthquakes and geodetic data. *Geophysical Journal International*, **160**, 217–226.

McQUARRIE, N. 2004. Crustal scale geometry of the Zagros fold–thrust belt, Iran. *Journal of Structural Geology*, **26**, 519–535.

McQUARRIE, N., STOCK, J. M., VERDEL, C. & WERNICKE, B. P. 2003. Cenozoic evolution of Neotethys and implications for the causes of plate motions. *Geophysical Research Letters*, **30**, 2036, doi: 10.1029/2003GL017992.

MERCIER, J.-L., CAREY-GAILHARDIS, E. & SÉBRIER, M. 1991. Palostress determinations from fault kinematics: Application to the Neotectonics of the Himalayas–Tibet and the central Andes. *Philosophical Transactions of the Royal Society of London*, **337**, 41–52.

MOLINARO, M., GUEZOU, J.-C., AUBOURG, C., LETURMY, P. & ESHRAGHI, S. A. 2003. Structural style across the Bandar Abbas syntaxis, SE Zagros: facts and factors of a subduction to collision transition. *EGS–AGU–EUG Joint Assembly, Nice*.

MOLINARO, M., GUEZOU, J. C., LETURMY, P., ESHRAGHI, S. A. & FRIZON DE LAMOTTE, D. 2004*a*. The origin of changes in structural style across the Bandar Abbas syntaxis, SE Zagros (Iran). *Marine and Petroleum Geology*, **21**, 735–752.

MOLINARO, M., LETURMY, P., GUEZOU, J.-C. & FRIZON DE LAMOTTE, D. 2004*b*. The structure and kinematic evolution of the south-eastern Zagros Mountains, Iran. *EGU 1st General Assembly, Nice*.

MOLINARO, M., LETURMY, P., GUEZOU, J.-C., FRIZON DE LAMOTTE, D. & ESHRAGHI, S. A. 2005. The structure and kinematics of the southeastern Zagros fold–thrust belt, Iran: From thin-skinned to thick-skinned tectonics. *Tectonics*, **24**, TC3007.

MOUTHEREAU, F., LACOMBE, O. & MEYER, B. 2006. The Zagros folded belt (Fars, Iran): constraints from topography and critical wedge modelling. *Geophysical Journal International*, **165**, 336–356.

MOUTHEREAU, F., TENSI, J., BELLAHSEN, N., LACOMBE, O., DE BOISGROLLIER, T. & KARGHAR, S. 2007*a*. Tertiary sequence of deformation in a thin-skinned/thick-skinned collision belt: the Zagros Folded Belt (Fars, Iran). *Tectonics*, **26**, TC5006.

MOUTHEREAU, F., LACOMBE, O., TENSI, J., BELLAHSEN, N., KARGAR, S. & AMROUCH, K. 2007*b*. Mechanical constraints on the development of the Zagros Folded Belt. *In*: LACOMBE, J. L. O., VERGÉS, J. & ROURE, F. (eds) *Thrust Belts and Foreland Basins: From Fold Kinematics to Hydrocarbon Sytems*. Frontiers in Earth Sciences. Springer, New York, 247–266.

NAVABPOUR, P., ANGELIER, J. & BARRIER, E. 2007. Cenozoic post-collisional brittle tectonic history and stress reorientation in the High Zagros Belt (Iran, Fars Province). *Tectonophysics*, **432**, 101–131.

OVEISI, B., LAVÉ, J. & VAN DER BEEK, P. A. 2007. Rates and processes of active folding evidenced by Pleistocene terraces at the central Zagros front (Iran). *In*: LACOMBE, O., LAVÉ, J., ROURE, F. & VERGÈS, J. (eds) *Thrust Belts and Foreland Basins*. Frontiers in Earth Sciences. Springer, New York, 265–285.

PARÉS, J. P., VAN DER PLUIJM, B. A. & DINARÈS-TURELL, J. 1999. Evolution of magnetic fabric during incipient deformation of mudrocks (Pyrenees, Northern Spain). *Tectonophysics*, **307**, 1–14.

REGARD, V., BELLIER, O., THOMAS, J. C., ABBASSI, M. R. & MERCIER, J. L. 2003. Tectonics of a lateral transition between subduction and collision: the Zagros–Makran transfer deformation zone (SE Iran). *In*: *EGS–AGU–EUG Joint Assembly, Nice*.

RICOU, L., BRAUD, J. & BRUNN, J. H. 1977. *Le Zagros*. Mémoires Hors Série de la Société Géologique de France, **8**, 33–52.

ROBION, P., GRELAUD, S. & FRIZON DE LAMOTTE, D. 2007. Pre-folding magnetic fabrics in fold-and-thrust belts: Why the apparent internal deformation of the sedimentary rocks from the Minervois basin (NE Pyrenees, France) is so high compared to the Potwar basin (SW Himalaya, Pakistan). *Sedimentary Geology*, **196**, 181–200.

ROCHETTE, P., JACKSON, J. & AUBOURG, C. 1992. Rock magnetism and the interpretation of ansisotropy of magnetic susceptibility. *Review of Geophysics*, **30**, 209–226.

ROWE, K. J. & RUTTER, E. H. 1990. Palaeostress estimation using calcite twinning: experimental calibration and application to nature. *Journal of Structural Geology*, **12**, 1–17.

SAGNOTTI, L., SPERENZA, F., WINKLER, A., MATTEI, M. & FUNICIELLO, R. 1998. Magnetic fabric of clay sediments from the external northern Apennines (Italy). *Physics of the Earth and Planetary Interiors*, **105**, 73–93.

SAINT-BEZAR, B., HEBERT, R. L., AUBOURG, C., ROBION, P., SWENNEN, R. & FRIZON DE LAMOTTE, D. 2002. Magnetic fabric and petrographic investigation of hematite-bearing sandstones within ramp-related folds: examples from the South Atlas Front (Morocco). *Journal of Structural Geology*, **24**, 1507–1520.

SATTARZADEH, Y., COSGROVE, J. W. & VITA-FINZI, C. 2000. The interplay of faulting and folding during the evolution of the Zagros deformation belt. *In*: COSGROVE, J. W. & AMEEN, M. S. (eds) *Forced Folds and Fractures*. Geological Society, London, Special Publications, **169**, 187–196.

SEPEHR, M. & COSGROVE, J. W. 2004. Structural framework of the Zagros Fold–Thrust, Iran. *Marine and Petroleum Geology*, **21**, 829–843.

SHERKATI, S. & LETOUZEY, J. 2004. Variation of structural style and basin evolution in the central Zagros (Izeh Zone and Dezful Embayment, Iran). *Marine and Petroleum Geology*, **21**, 535–554.

SHERKATI, S., MOLINARO, M., FRIZON DE LAMOTTE, D. & LETOUZEY, J. 2005. Detachment folding in the central and eastern Zagros fold-belt (Iran): salt mobility, multiple detachment and final basement control. *Journal of Structural Geology*, **27**, 1680–1696.

SHERKATI, S., LETOUZEY, J. & FRIZON DE LAMOTTE, D. 2006. Central Zagros fold–thrust belt (Iran): new insights from seismic data, field observation, and sandbox modeling. *Tectonics*, **25**, TC4007, doi: 10.1029/2004TC001766.

SMITH, B., AUBOURG, C., GUÉZOU, J. C., NAZARI, H., MOLINARO, M., BRAUD, X. & GUYA, N. 2005. Kinematics of a sigmoidal fold and vertical axis rotation in the east of the Zagros–Makran syntaxis (Southern

Iran): palaeomagnetic, magnetic fabric and microtectonic approaches. *Tectonophysics*, **411**, 89–109.

TALEBIAN, M. & JACKSON, J. 2004. A reappraisal of earthquake focal mechanisms and active shortening in the Zagros mountains of Iran. *Geophysical Journal International*, **156**, 506–526.

TARLING, D. H. & HROUDA, F. 1993. *The Magnetic Anisotropy of Rocks*. Chapman & Hall, London.

TATAR, M., HATZFELD, D., MARTINOD, J., WALPERSDORF, A., GHAFORI-ASHTIANY, M. & CHÉRY, J. 2002. The present-day deformation of the central Zagros from GPS measurements. *Geophysical Research Letters*, **29**, 19–27.

TATAR, M., HATZFELD, D. & GHAFORY-ASHTIANY, M. 2004. Tectonics of the Central Zagros (Iran) deduced from microearthquake seismicity. *Geophysical Journal International*, **156**, 255–266.

VERNANT, P., NILFOROUSHAN, F. *ET AL*. 2004. Present-day crustal deformation and plate kinematics in the Middle East constrained by GPS measurements in Iran and northern Oman. *Geophysical Journal International*, **157**, 381–398.

WALPERSDORF, A., HATZFELD, D. *ET AL*. 2006. Difference in the GPS deformation pattern of North and Central Zagros (Iran). *Geophysical Journal International*, **167**, 1077–1088.